Radiative flavor template at the LHC: $g-2$ and the W mass

Giacomo Cacciapaglia,[1,2,*] Antimo Cagnotta,[3,4,†] Roberta Calabrese,[3,4,‡] Francesco Carnevali,[3,4,§] Agostino De Iorio,[3,4,‖] Alberto Orso Maria Iorio,[3,4,¶] Stefano Morisi,[3,4,**] and Francesco Sannino[3,4,5,6,††]

[1]*Institut de Physique des 2 Infinis de Lyon (IP2I), UMR5822, CNRS/IN2P3, F-69622 Villeurbanne Cedex, France*
[2]*University of Lyon, Université Claude Bernard Lyon 1, F-69001 Lyon, France*
[3]*Dipartimento di Fisica "Ettore Pancini," Università degli studi di Napoli "Federico II," Complesso Univ. Monte S. Angelo, I-80126 Napoli, Italy*
[4]*INFN—Sezione di Napoli, Complesso Univ. Monte S. Angelo, I-80126 Napoli, Italy*
[5]*Scuola Superiore Meridionale, Largo S. Marcellino, 10, 80138 Napoli NA, Italy*
[6]*CP^3-Origins and Danish-IAS, Univ. of Southern Denmark, Campusvej 55, 5230 Odense M, Denmark*

(Received 6 January 2023; accepted 27 February 2023; published 21 March 2023)

The Standard Model of particle physics and its description of nature have been recently challenged by a series of precision measurements performed via different accelerator machines. Statistically significant anomalies emerged when measuring the muon magnetic momentum, and very recently when deducing the mass of the $\mathcal{W}$ boson. Here we consider a radiative extension of the Standard Model devised to be sufficiently versatile to reconcile the various experimental results while further predicting the existence of new bosons and fermions with a mass spectrum in the TeV energy scale. The resulting spectrum is, therefore, within the energy reach of the proton-proton collisions at the LHC experiments at CERN. The model investigated here allows us to interpolate between composite and elementary extensions of the Standard Model with an emphasis on a new modified Yukawa sector that is needed to accommodate the anomalies. Focusing on the radiative regime of the model, we introduce interesting search channels of immediate impact for the ATLAS and CMS experimental programs such as the associate production of Standard Model particles with either invisible or long-lived particles. We further show how to adapt earlier supersymmetry-motivated searchers of new physics to constrain the spectrum and couplings of the new scalars and fermions. Overall, the new physics template simultaneously accounts for the bulk of the observed experimental anomalies while suggesting a wide spectrum of experimental signatures relevant for the current LHC experiments.

DOI: 10.1103/PhysRevD.107.055033

I. INTRODUCTION

In the first two decades of this millennium, increasing experimental evidence of the existence of new physics (NP) beyond the Standard Model (SM) has been accumulated. Several standard deviations from the SM predictions have been observed when determining the anomalous magnetic moment $(g-2)$ of the muon by the E821 experiment [1] at Brookhaven National Laboratory, and in the semileptonic decays $B \to D^{(*)} l\nu$ [2–4] and $B \to K^{(*)} ll$ [5] by the *BABAR*, Belle, and LHCb Collaborations. These anomalies have been confirmed by the most recent measurement performed by the Muon $g-2$ Collaboration at Fermilab [6] and at flavor experiments [7,8]. Notably, the anomalies in the semileptonic B meson decays emerge due to the observed differences between the decay rates in different lepton families, encoded in the ratios $R_{K^{(*)}}$ and $R_{D^{(*)}}$. In the third decade of this century, the CDF II Collaboration at Fermilab offered an unexpected sign of new physics by unveiling the high-precision measurement of the $\mathcal{W}$ boson mass [9] from decade-old Tevatron data. The result is 7 standard deviations away from the SM prediction. Even after taking into account higher-order corrections [10] and the proper average with previous measurements [11,12],

*g.cacciapaglia@ip2i.in2p3.fr
†antimo.cagnotta@unina.it
‡rcalabrese@na.infn.it
§francesco.carnevali@unina.it
‖agostino.deiorio@unina.it
¶albertoorsomaria.iorio@unina.it
**smorisi@na.infn.it
††sannino@cp3.sdu.dk

which reduce the tension to a little less than 4 standard deviations [12,13], this result clearly points toward a tension with the SM [14–16]. The most recent LHCb results [17,18] do, however, show a compatibility of $R_{K^{(*)}}$ with the SM within 2 standard deviations. All this evidence [12] adds to long-standing indirect hints of NP, most notably the dark matter problem, the origin of neutrino masses that emerge from the observation of neutrino oscillations, and the origin of the baryon asymmetry in the Universe.

Models with additional fermions and scalars, which couple to a single SM quark or lepton via new Yukawa-like couplings not involving the SM Brout-Englert-Higgs field, are prime candidates to explain the $g-2$ anomalies while taking into account the B meson data [19–25]. The NP contributions arise at loop level, while additional bounds come, most notably, from B_0–$\bar{B}_0$ mixing and effects on the Z and Higgs bosons couplings to muons. Such models, depending on the quantum numbers of the new states, can also contain a dark matter candidate [23]. A model of this kind has been used in Ref. [26] as a template interpolating perturbative models and strongly interacting models, like technicolorlike ones and models of fundamental partial compositeness [27–29]. In the latter limit, the multiplicity of the new fermions and scalars is due to a new confining gauge interaction. The inclusion of the $R_{D^{(*)}}$ anomalies in this class of models requires further investigation, as loop effects can hardly compete with the tree-level contribution to the $B \to D^{(*)} l\nu$ decay processes in the SM. Corrections to the $\mathcal{W}$ boson mass can also be explained in the context of this model as coming from additional fermion loops, providing additional constraints on the new particles and couplings.

In this paper, we aim to describe the productions and decays of the new families of bosons and fermions in proton-proton collisions, in the conditions akin to the ones provided by the Large Hadron Collider (LHC) and future hadron collider projects. We will, in particular, estimate the limits on the parameter space from current LHC searches and identify promising new channels that deserve further investigation and dedicated searches.

We focus on the radiative case, where the new fermions and scalars can be directly produced. In the composite case, they are confined in new meson and baryon states that need to be studied at the LHC via their effective interactions.

This article is structured as follows: Section II gives a brief overview of the framework following the notation adopted in Ref. [26], establishing the terminology and the assumptions made in the rest of the paper. Section III describes the signatures that could arise in proton-proton collisions, following different hypotheses on the mass hierarchies and on the parameter range allowed by the precision measurement constraints, while Sec. IV focuses on describing in detail the phenomenological implications at the LHC of one specific decay channel via the reinterpretation of one existing search by the Compact Muon Solenoid (CMS) experiment. Finally, Sec. V reviews the constraints on the anomalies in the context of this model and draws conclusions on the potential for future studies at the LHC, before the conclusions in Sec. VI.

II. THEORETICAL FRAMEWORK

Following Ref. [26], the class of models described here naturally interpolates between dynamical models of electroweak symmetry breaking and perturbative models where radiative corrections contribute to flavor observables. In the latter case, the new strong gauge symmetry is demoted to a global one, acting on the new fermions and scalars, hence simply counting their multiplicity. The main contribution to anomalies, therefore, stems from loop diagrams involving the new fermions and scalars. These loops also contribute to the Yukawa couplings of the SM fermions; hence, one can design models where light fermion masses and flavor structures can be radiatively generated [30]. In this work, we will consider a more general scenario, where direct couplings of the SM fermions to the Higgs boson are also present, and SM fermion masses emerge from a combination of the tree-level couplings and the loop contributions. For concreteness, we will consider a model where the SM is extended by means of a set of Dirac fermions, an $SU(2)_L$ doublet $\mathcal{F}_L$ and two $SU(2)_L$ singlets $\mathcal{F}_N$ and $\mathcal{F}_E$, and two scalar fields $\mathcal{S}_\ell$ and $\mathcal{S}_q$. Their assigned quantum numbers are shown in Table I. We can appreciate that the hypercharge of these new fundamental particles is fixed once the parameter Y is chosen. Integer values of Y for the radiative case are not allowed, because they would lead to fractionally charged elementary states, and $|Y| > 1/2$ are not allowed because they would not admit neutral particles.

In this paper we will focus our attention on the case $Y = 1/2$ [26].

The NP resides in the Yukawa sector of the theory by means of the most general Yukawa Lagrangian involving the new fermions that is also, by construction, invariant under the global $\mathcal{G}_{TC}$ symmetry. Besides kinetic terms and masses for the new fermions and scalars, the SM Lagrangian is complemented by the following set of Yukawa-like interactions:

$$\begin{aligned} -L_{\mathrm{Yuk,NP}} = {} & y_L^{ij} L^i \mathcal{F}_L (\mathcal{S}_E^j)^* + y_E^{ij} (E^i)^c \mathcal{F}_N^c \mathcal{S}_E^j \\ & + y_Q^{ij} Q^i \mathcal{F}_L (S_D^j)^* \\ & + y_D^{ij} (D^i)^c \mathcal{F}_N^c \mathcal{S}_D^j + y_U^{ij} (U^i)^c \mathcal{F}_E^c \mathcal{S}_D^j \\ & + \sqrt{2} (k_\uparrow \mathcal{F}_L \mathcal{F}_N^c + k_\downarrow \mathcal{F}_E \mathcal{F}_L^c) \Phi_H + \mathrm{H.c.}, \end{aligned} \quad (1)$$

where $\mathcal{F}_L = (\mathcal{F}_L^\uparrow, \mathcal{F}_L^\downarrow)^{\mathrm{T}}$ with respect to $SU(2)_L$ while Q, U^c, D^c, L, E^c are the SM fermions expressed in terms of chiral left-handed spinors. Note also that the SM flavor indices i, j are carried by the scalars. The field Φ_H is the

TABLE I. Quantum numbers of the additional fermions $\mathcal{F}$ and scalars $\mathcal{S}$ as in Ref. [26]. Note that $\mathcal{G}_{TC}$ is a global symmetry in our scenario, while $j = 1, 2, 3$ is a family index. The nomenclature follows the association of $\mathcal{F}_E$ with the down-component of the doublet, similar to electrons in the SM (and analogously for $\mathcal{F}_N$). Charges similar to the SM ones are obtained for $Y = -1/2$, as shown in the last column. In this paper, however, we will study the case $Y = 1/2$, as shown in the second-to-last column.

	$\mathcal{G}_{TC}$	$SU(3)_c$	$SU(2)_L$	$U(1)_Y$	$Q(Y=1/2)$	$Q(Y=-1/2)$
$\mathcal{F}_L = \begin{pmatrix} \mathcal{F}_L^{\uparrow} \\ \mathcal{F}_L^{\downarrow} \end{pmatrix}$	$\mathbf{F}$	1	2	Y	$\begin{pmatrix} +1 \\ 0 \end{pmatrix}$	$\begin{pmatrix} 0 \\ -1 \end{pmatrix}$
${\mathcal{F}_N}^c$	$\bar{\mathbf{F}}$	1	1	$-Y-1/2$	-1	0
${\mathcal{F}_E}^c$	$\bar{\mathbf{F}}$	1	1	$-Y+1/2$	0	1
$\mathcal{S}_\ell^j$	$\mathbf{F}$	1	1	$Y-1/2$	0	-1
$\mathcal{S}_q^j$	$\mathbf{F}$	3	1	$Y+1/6$	$+\frac{2}{3}$	$-\frac{1}{3}$

SM Higgs scalar doublet. The complete Lagrangian also contains a generic scalar potential to complement the usual SM Lagrangian. Also, the fields R^c transform as the representation conjugated to R, for example, $U^c = (\bar{3}, 1)_{-2/3}$. Further terms that violate $\mathcal{G}_{TC}$ can be added to Eq. (1), and they will be considered in a follow-up work.

For the choice $Y = 1/2$ we made in this analysis, the electric charges of the new fermions and scalars are fixed, as reported in Table I. We see that $\mathcal{S}_q$ has the same charge as up-type quarks, while $\mathcal{F}_L^{\downarrow}$ and $\mathcal{F}_E$ are neutral, and $\mathcal{F}_L^{\uparrow}$ and $\mathcal{F}_N$ carry positive charge. This implies, for instance, that $\mathcal{S}_q^j$ can decay into an up-type quark plus a neutral heavy fermion or a down-type quark and a heavy charged fermion. This will be further explored in Sec. III, where a detailed description of the experimental signatures will be given. The scalars $\mathcal{S}_\ell^j$ are also neutral: Since, in the absence of $\mathcal{G}_{TC}$-violating operators the new fermions and scalars cannot decay into SM states, we need the lightest state to be neutral and, therefore, act as a potential dark matter candidate. Having fixed Y, the remaining parameters of the model are the Yukawa matrices $y^{ij}_{Q,U,D}$, $y^{ij}_{L,E}$, the couplings $k_{\uparrow,\downarrow}$, and the masses of the new scalars and fermions.

III. SIGNATURES IN PROTON-PROTON COLLISIONS

Constraints on NP scenarios coming from heavy meson physics and electroweak (EW) precision measurements can be complemented by direct searches at the LHC. In our radiative model, the masses of the new fermions and scalars are preferably above the EW scale, hence, spanning from a few hundred GeV to a few TeV. As the fermions $\mathcal{F}$ and the scalar $\mathcal{S}_\ell$ are colorless, their production at proton-proton colliders will be very small. On the contrary, the $\mathcal{S}_q$ scalars carry color charge; hence, they are produced via gluon and quark fusion, $gg \to \mathcal{S}_q\mathcal{S}_q^*$ and $q\bar{q} \to \mathcal{S}_q\mathcal{S}_q^*$ in proton-proton collisions via QCD interactions. Representative leading-order Feynman diagrams for pair $\mathcal{S}_q$ production are shown in Fig. 1. This kind of production mechanism has a limited dependence on the parameters of the model. Since the color charge and the spin of $\mathcal{S}_q$ are set, the pair production cross section only depends on the mass $m_{\mathcal{S}_q}$ of the new boson and on the multiplicity: namely, N_{TC} and the number of light families. Direct production of a single $\mathcal{S}_q$ boson accompanied by one $\mathcal{F}_L$ or $\mathcal{F}_E/\mathcal{F}_N$ fermion is also possible with representative leading-order Feynman diagrams shown in Fig. 2. In this case, a NP interaction vertex, e.g., $Q\mathcal{S}_q\mathcal{F}_L$, is necessarily involved; hence, the parton-level cross section depends on the details of the models and on the NP couplings. In particular, left-handed production will depend on the coupling y_Q^{ij}, while right-handed production will depend on y_U^{ij}, y_D^{ij}.

This section will cover possible experimental signatures coming from pair production of $\mathcal{S}_q$ bosons, and we will focus on the minimal scenario where only one $\mathcal{S}_q$ family is present (and all others are heavier). The experimental signatures of $\mathcal{S}_q$ boson pairs produced at the LHC depend on the decay chains allowed within the model. The particular realization of the model described in Sec. II is not fully determined by the precision measurements, which are detailed in Appendix A. In fact, it is the mass of the boson $m_{\mathcal{S}_q}$, the masses of both up-type and down-type fermions $m_{\mathcal{F}_L^{\uparrow}}$ and $m_{\mathcal{F}_L^{\downarrow}}$, the other fermions $\mathcal{F}_E$ and $\mathcal{F}_N$, as well as the coupling strengths that will determine the

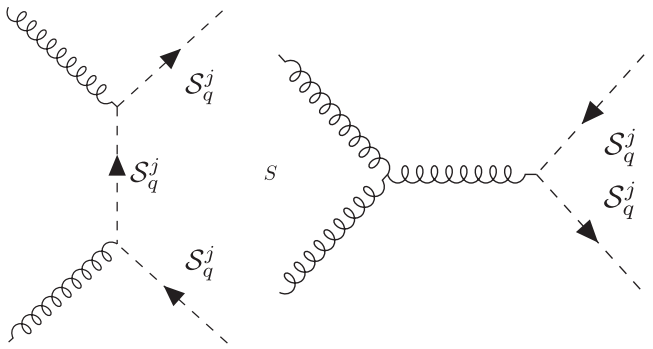

FIG. 1. Representative leading-order Feynman diagrams for pair $\mathcal{S}_q$ production.

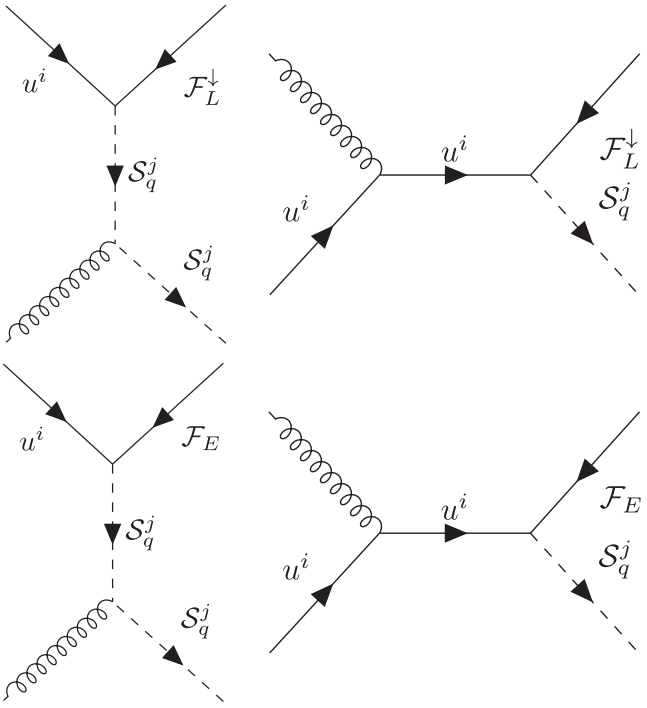

FIG. 2. Representative leading-order Feynman diagrams for $\mathcal{S}_q$ plus $\mathcal{F}$ production.

possible decays for the $\mathcal{S}_q$ bosons and the respective branching fractions. We describe these final states in two steps: In the first step, we address the direct decays of the $\mathcal{S}_q$ boson, which depend on the coupling strengths, i.e., y_Q^{ij}, y_U^{ij}, and y_D^{ij}, and on the difference in mass between $\mathcal{S}_q$ and the fermions. In the second step, we will describe the possible decay cascades and final states that can arise depending on the mass hierarchy between the various fermions $\mathcal{F}$ and $\mathcal{S}_\ell$. In Sec. IV, we will describe the example of one particular realization that can be used to derive quantitative predictions at the LHC.

A. Decays of the $\mathcal{S}_q$ bosons and the flavor basis

To properly discuss the phenomenology stemming from $\mathcal{S}_q$ pair production, we first need to bring the interactions in Eq. (1) to the mass eigenstate basis. For the scalars, we can assume without loss of generality that the mass matrices are already diagonal; hence, selecting the lightest state consists of fixing the index j in the couplings. In the heavy fermion sector, instead, a mixing is generated by the couplings to the Higgs $k_\uparrow$ and $k_\downarrow$. This mixing is proportional to the EW scale versus the vectorlike mass of the $\mathcal{F}$ fermions; hence, it is typically small. In the following, mainly for simplicity, we will neglect mixing effects.

In the quark sector, instead, the flavor mixing cannot be neglected as it plays a crucial role in determining the flavor structure in the $\mathcal{S}_q$ coupling. The masses receive a contribution both from a SM-like Yukawa coupling and from loops of the new fermions and scalars, similar to the muon mass sketched in Appendix A 1. Hence, the masses to be diagonalized for up- and down-type quarks read

$$M_u^{ik} = \frac{(y_u^{\rm SM})^{ik} v}{\sqrt{2}} + N_{TC} \sum_{j=1}^{3} \frac{(y_Q^{ij} y_U^{kj})}{16\pi^2} \frac{k_\uparrow v}{\sqrt{2}} F_{\rm loop}(M_{\mathcal{S}_q}^j, \text{masses}), \tag{2}$$

$$M_d^{ik} = \frac{(y_d^{\rm SM})^{ik} v}{\sqrt{2}} + N_{TC} \sum_{j=1}^{3} \frac{(y_Q^{ij} y_D^{kj})}{16\pi^2} \frac{k_\downarrow v}{\sqrt{2}} F_{\rm loop}(M_{\mathcal{S}_q}^j, \text{masses}). \tag{3}$$

The diagonalization leading to the mass eigenstates, i.e., to the SM quarks, derives from a nontrivial interplay between the SM-like Yukawas and the loop contributions. In general, the flavor structure in the mass matrices is not aligned to the one of the new couplings $y_{Q,U,D}$. In the mass eigenstate basis, the Yukawa couplings $y_{Q,U,D}$ are rotated by unphysical rotation matrices, which cannot be measured independently from the Yukawa couplings themselves. In the following, we consider the matrices in the mass eigenstate basis without changing the notation for simplicity. Like in the SM, the only rotation matrix that is physical is the Cabibbo-Kobayashi-Maskawa (CKM) one deriving from a different rotation of the up and down components of the left-handed fields. The couplings of $\mathcal{S}_q^j$ in the mass eigenstate basis, therefore, read

$$q_{uL} \mathcal{F}_L^\downarrow (\mathcal{S}_q^j)^* \Rightarrow y_Q^{qj} \quad q_u = u, c, t, \tag{4}$$

$$q_{dL} \mathcal{F}_L^\uparrow (\mathcal{S}_q^j)^* \Rightarrow \sum_a V_{qa} y_Q^{aj} \qquad q_d = d, s, b, \tag{5}$$

$$q_{uR}^c \mathcal{F}_E{}^c \mathcal{S}_q^j \Rightarrow y_U^{qj} \quad q_u = u, c, t, \tag{6}$$

$$q_{dR}^c \mathcal{F}_N{}^c \mathcal{S}_q^j \Rightarrow y_D^{qj} \quad q_d = d, s, b, \tag{7}$$

where we follow the convention that the CKM rotation is assigned to the couplings of the left-handed down-type quarks.

The first step of the $\mathcal{S}_q$ decays is induced by the couplings above, as illustrated in Fig. 3. In the following, we will assume that the couplings y_Q are much larger than $y_{U,D}$; hence, we will only consider the decays in the upper diagrams, which involve the doublet fermions $\mathcal{F}_L^\uparrow$ and $\mathcal{F}_L^\downarrow$. The reason for this choice is twofold: On the one side, the products $y_Q y_U$ and $y_Q y_D$ control the loop correction to the quark masses and they need to be small for light quarks (see also discussion on the muon mass); on the other hand, the constraints discussed in Appendix A prefer larger contributions in the left-handed sector. Henceforth, the partial decay widths of $\mathcal{S}_q$ into up- or down-type quarks are given by

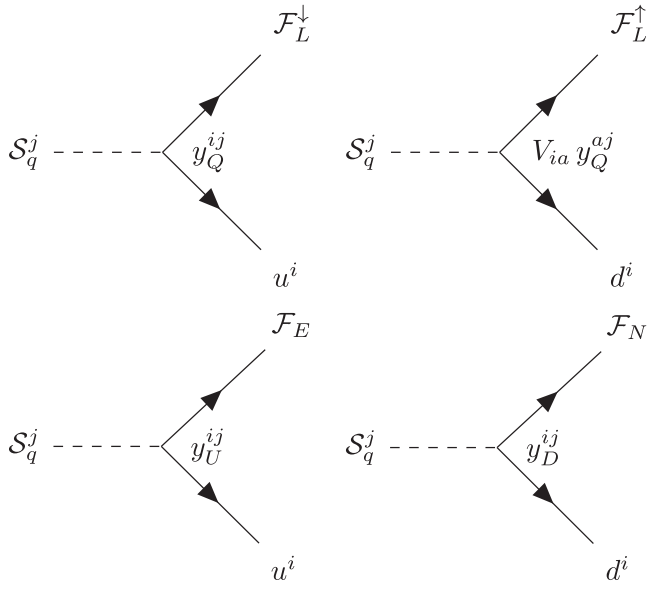

FIG. 3. Decay vertices for $\mathcal{S}_q$ bosons to left-handed (top panels) or right-handed (bottom panels) new fermions and an up-type (left panels) or down-type (right panels) quark.

$$\Gamma^j_{q_u} \equiv |y_Q^{qj}|^2 \cdot \frac{m_{\mathcal{S}_{q\,j}}{}^2 - (m_{\mathcal{F}_L^{\downarrow}} - m_{q_u})^2}{32\pi \cdot m_{\mathcal{S}_{q\,j}}{}^3} \cdot (m_{\mathcal{S}_{q\,j}}{}^2 - m^2_{\mathcal{F}_L^{\downarrow}} - m^2_{q_u}), \tag{8}$$

$$\Gamma^j_{q_d} \equiv \left|\sum\nolimits_k V_{qk} y_Q^{kj}\right|^2 \cdot \frac{m_{\mathcal{S}_{q\,j}}{}^2 - (m_{\mathcal{F}_L^{\uparrow}} - m_{q_d})^2}{32\pi \cdot m_{\mathcal{S}_{q\,j}}{}^3} \cdot (m_{\mathcal{S}_{q\,j}}{}^2 - m^2_{\mathcal{F}_L^{\uparrow}} - m^2_{q_d}). \tag{9}$$

Defining the total width of $\mathcal{S}_q^j$ as

$$\Gamma^j = \sum_{q_u=u,c,t} \Gamma^j_{q_u} + \sum_{q_d=d,s,b} \Gamma^j_{q_d}, \tag{10}$$

the branching ratios into different quark flavors read

$$\mathrm{BR}(q_u, \mathcal{F}_L^{\downarrow}) = \frac{\Gamma^j_{q_u}}{\Gamma^j}, \qquad q_u = u, c, t, \tag{11}$$

$$\mathrm{BR}(q_d, \mathcal{F}_L^{\uparrow}) = \frac{\Gamma^j_{q_d}}{\Gamma^j}, \qquad q_d = d, s, b. \tag{12}$$

More general formulas, including all the mixing patterns, can be obtained in a straightforward way.

B. Chain decays and detector signatures

The decay cascades of the $\mathcal{F}_L$, $\mathcal{F}_E$, and $\mathcal{F}_N$ produced in the decays of the $\mathcal{S}_q$ bosons depend on the respective masses and the mass of $\mathcal{S}_\ell$. For simplicity, in the following discussion we will assume that $\mathcal{F}_N$ and $\mathcal{F}_E$ are heavier than $\mathcal{F}_L$, as they do not appear in the decays following the left-handed coupling dominance. In particular, if $\mathcal{F}_L^{\uparrow}$ is the lightest particle of the model, it will not further decay and, being charged, it will appear as a long-lived charged particle (LLCP). We are implicitly assuming that it will decay via a suppressed higher-order operator in SM states (leptons) outside the detector, as it cannot be stable on cosmological timescales. Instead, if $\mathcal{F}_L^{\downarrow}$ is the lightest particle, being neutral it will result in missing momentum and energy in the detector that we will henceforth shorten as "MET." Note also that the mass hierarchy between $\mathcal{F}_L^{\uparrow}$ and $\mathcal{F}_L^{\downarrow}$ plays a crucial role: The heavier one will decay into the lighter via a real or virtual $\mathcal{W}$ boson. In fact, the two components of the doublet cannot be degenerate. Reproducing the anomaly in the W mass measurement requires a mass split of a few tens of GeV. Even if the mass split vanishes at tree level (for $k_\uparrow = k_\downarrow$), one is induced by EW loops, and it amounts to roughly 166 MeV in the large mass limit [31], and it is enough to generate a prompt decay of the heavier into the lightest (plus a charged pion) [32]. Finally, the neutral scalars $\mathcal{S}_\ell^j$ couple to $\mathcal{F}_L$ via the coupling y_L; hence, if it is lighter than $\mathcal{F}_L^{\uparrow}$ and $\mathcal{F}_L^{\downarrow}$, the fermions will decay into it, producing missing energy plus a lepton. We assume that the lightest $\mathcal{S}_\ell^j$ can be stable and produce MET.

The possible decay chains of the fermions $\mathcal{F}_L^{\uparrow}$ and $\mathcal{F}_L^{\downarrow}$ are described in the following, depending on the mass ordering, and refer to Feynman diagrams shown in Figs. 3 and 4. We distinguish the following cases:

(1) $m_{\mathcal{S}_\ell} > m_{\mathcal{F}_L^{\uparrow}}, m_{\mathcal{F}_L^{\downarrow}}$: The fermions are the lightest particles, but one fermion will decay into the other plus a $\mathcal{W}$ boson, either virtual or real. States with either MET or LLCPs are possible, depending on which fermion is the lightest. Representative diagrams for this case are the ones in Figs. 3 and 4, first row.

(2) $m_{\mathcal{S}_\ell} < m_{\mathcal{F}_L^{\uparrow}}, m_{\mathcal{F}_L^{\downarrow}}$: The neutral scalar $\mathcal{S}_\ell$ is the lightest particle, and final states involve missing energy from $\mathcal{S}_\ell$ plus at least one lepton, either charged or neutral, from the NP vertex involving $\mathcal{S}_\ell$ and $\mathcal{F}_L$. Representative diagrams for this case are the ones in Fig. 4, second row.

(3) $m_{\mathcal{S}_\ell} < m_{\mathcal{F}_L^{\uparrow}}, m_{\mathcal{F}_L^{\downarrow}}$: The scalar $\mathcal{S}_\ell$ is the lightest particle, and final states involve missing energy from the $\mathcal{S}_\ell$ plus at least one lepton from from the NP vertex involving the $\mathcal{S}_\ell$ and the $\mathcal{F}_L$ or $\mathcal{F}_N$. In this case, one fermion will decay in the other one plus a $\mathcal{W}$ boson. Representative diagrams for this case are the ones in Fig. 4, third row.

(4) $m_{\mathcal{F}_L^{\downarrow}} < m_{\mathcal{S}_\ell} < m_{\mathcal{F}_L^{\uparrow}}$ or $m_{\mathcal{F}_L^{\uparrow}} < m_{\mathcal{S}_\ell} < m_{\mathcal{F}_L^{\downarrow}}$: In this case, one of the fermions can decay into the $\mathcal{S}_\ell$ that further cascades into the second type of fermion plus a lepton, respectively, charged or neutral for the two cases.

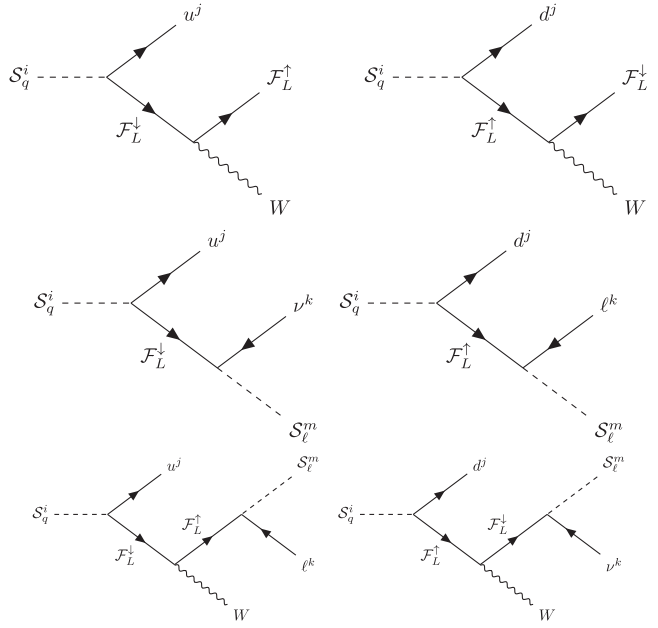

FIG. 4. Decay vertices for $\mathcal{S}_q$ bosons to left-handed (top panels) or right-handed (bottom panels) new fermions and an up-type (left panels) or down-type (right panels) quark.

It is worthy of note that the difference in mass between the up-type and down-type fermion $|m_{\mathcal{F}_L^\uparrow} - m_{\mathcal{F}_L^\downarrow}|$ needs to be sizeable and in the range of tens of GeV in order to account for the $m_{\mathcal{W}}$ measurement, as shown in Appendix A 5. Moreover, $|m_{\mathcal{F}_L^\uparrow} - m_{\mathcal{F}_L^\downarrow}| < m_{\mathcal{W}}$ for the largest part of the parameter space, so the $\mathcal{W}$ boson produced in the decays will be virtual in most of the cases. For most parameter choices, $m_{\mathcal{S}_\ell}$ is significantly different from $m_{\mathcal{F}_L^\uparrow}$ and $m_{\mathcal{F}_L^\downarrow}$; therefore, scenario 4 from the above list is also unlikely to occur.

Table II summarizes all possible decay chains depending on the mass hierarchy.

Finally, a note for the $Y = -1/2$ scenario: While the diagrams are the same as the $Y = 1/2$ case, the quantum numbers of the particles are different, as reported in the last column of Table I. This has the consequence that final states still involve either MET or LLCPs, but in this case, an $\mathcal{F}_L^\uparrow$ contributes to the MET, while an $\mathcal{F}_L^\downarrow$ or an $\mathcal{S}_\ell$ manifests as a LLCP.

IV. CONSTRAINTS FROM LHC DIRECT SEARCHES

In order to derive quantitative predictions for observable quantities at the LHC, the model needs to be fully specified, including the coupling structure and the mass hierarchy. In the following, we first describe the scenarios with the minimum number of parameters necessary for explaining the anomalies in muon $g-2$ and $m_{\mathcal{W}}$, while accounting for the B meson sector constraints, then we describe the final states and compare them to existing analyses at the LHC. We focus on the scalars $\mathcal{S}_q$, as discussed in the previous section, which have the same quantum numbers as the (right-handed) stop in supersymmetry (SUSY); hence, we will focus on SUSY searches that are very close to our expected signal.

A. Minimal scenarios

In the models described in Sec. II, only the left-handed couplings to quarks are explicitly needed. The minimal benchmark scenario therefore requires both right-handed couplings to quarks being zero. Hence, our "minimal scenario" consists of nonvanishing y_Q^{ij} and y_L^{ij}, while the other Yukawas are negligible [33]. Furthermore, we will consider only one of the $\mathcal{S}_q$ to be light, corresponding to preferential couplings to the third generation of SM fermions.

In this section, we will consider this scenario where there is only one value for $j = 3$ to reflect that the lightest $\mathcal{S}_q$ couples preferably to the third-generation quarks. The constraint in the quark sector comes from the coupling between mass eigenstates referred to as $(y_Q y_Q^\dagger)_{bs}$ in Appendix A, which would hint at a preferential coupling to second and third quark generation. A first so-called "natural" minimal scenario (NMS), therefore, foresees $y_Q^{13} = 0$, $y_Q^{23} \neq 0$, and $y_Q^{33} \neq 0$. By using the Wolfenstein parametrization for the CKM matrix, it is possible to write the contributions coming from different mass eigenstates as in powers of λ, and by neglecting λ^4 terms, one finds

TABLE II. Description of the possible decays at the LHC depending on the mass hierarchy of the particles.

	$m_{\mathcal{S}_\ell} > m_{\mathcal{F}_L^\uparrow}, m_{\mathcal{S}_\ell} > m_{\mathcal{F}_L^\downarrow}$	$m_{\mathcal{S}_\ell} < m_{\mathcal{F}_L^\uparrow}, m_{\mathcal{S}_\ell} < m_{\mathcal{F}_L^\downarrow}$	$m_{\mathcal{F}_L^\downarrow} < m_{\mathcal{S}_\ell} < m_{\mathcal{F}_L^\uparrow}$[a]	$m_{\mathcal{F}_L^\uparrow} < m_{\mathcal{S}_\ell} < m_{\mathcal{F}_L^\downarrow}$[a]
$m_{\mathcal{F}_L^\uparrow} > m_{\mathcal{F}_L^\downarrow}$	MET $+ u$, MET $+ \mathcal{W} + d$	MET $+ u$, MET $+ \mathcal{W} + d$, MET $+ d + l$	MET $+ u$, MET $+ d$, MET $+ d + l$	NA
$m_{\mathcal{F}_L^\downarrow} > m_{\mathcal{F}_L^\uparrow}$	LLCP $+ d$ LLCP $+ d + \mathcal{W}$	MET $+ u$ MET $+ \mathcal{W} + l$	NA	MET $+ u +$ LLCP $+ l$ MET $+ u + \mathcal{W} +$ LLCP

u,d are the up- or down-type quark of the ith family; l is the charged lepton; $\mathcal{W}$ is the $\mathcal{W}$ boson.
[a]Limited phase space: $m_{\mathcal{F}} \gtrsim 1$ TeV.

TABLE III. Description of the minimal scenarios considered.

	Minimal scenarios	
Parameter	Natural (NMS)	Democratic (DMS)
Number of $\mathcal{S}_q$	$1 \times N_{TC}$	$1 \times N_{TC}$
Couplings	$y_Q^{13} = 0;\ y_Q^{23} \neq 0;\ y_Q^{33} \neq 0$	$y_Q^{13} \neq y_Q^{23} \neq y_Q^{33}$
$(y_Q y_Q^\dagger)_{bs}$	$A\lambda^2 (y_Q^{33})^2 + y_Q^{33} y_Q^{23} + A\lambda^2 (y_Q^{23})^2$	$A\lambda^2 (y_Q^{33})^2 + y_Q^{33}(y_Q^{23} + \lambda y_Q^{13}) + A\lambda^2 (y_Q^{23} + \lambda y_Q^{13})^2$

$$(y_Q y_Q^\dagger)_{bs} \equiv \sum_{i,k=1}^{3} V_{bi} (y_Q)_{i3} (y_Q^\dagger)_{3k} V_{ks}^\dagger = A\lambda^2 (y_Q^{33})^2 + y_Q^{33} y_Q^{23} + A\lambda^2 (y_Q^{23})^2. \quad (13)$$

Another possibility we consider is the "democratic" minimal scenario (DMS), where all three couplings are different. By neglecting orders λ^3 or higher, one finds

$$(y_Q y_Q^\dagger)_{bs} = A\lambda^2 (y_Q^{33})^2 + y_Q^{33}(y_Q^{23} + \lambda y_Q^{13}) + A\lambda^2 (y_Q^{23} + \lambda y_Q^{13})^2. \quad (14)$$

It is noteworthy that, in the NMS, decays to first-generation quarks will only be present via CKM mixing, hence strongly suppressed. In the DMS, instead, coupling to first-generation quarks will be present and not necessarily small, and they contribute to the final states to consider when obtaining constraints on the model. In the following, we will make use of Eqs (13) and (14) in order to impose the constraint on $(y_Q y_Q^\dagger)_{bs}$ from the $B_0 - \bar{B}_0$ mass mixing and derive the constraint on the branching fractions.

Table III summarizes the parameters in the considered scenario.

B. Squarklike final states: Quark pairs + missing energy

The particular final states that will be detected at a hadron collider, like the LHC, depend on the decays that are possible, and ultimately on the mass hierarchy of the new particles, as described in Sec. III. If we consider as a benchmark a simple scenario where $m_{\mathcal{S}_\ell} > m_{\mathcal{F}_L^\uparrow}$, $m_{\mathcal{S}_\ell} > m_{\mathcal{F}_L^\downarrow}$, and $m_{\mathcal{F}_L^\downarrow} > m_{\mathcal{F}_L^\uparrow}$, then each $\mathcal{S}_q$ can decay either to an up-type quark plus $\mathcal{F}_L^\downarrow$, or a down-type quark plus $\mathcal{F}_L^\uparrow$. The latter further decays to $\mathcal{F}_L^\downarrow$ plus a virtual $\mathcal{W}$ boson. Hence, the detector signatures for a single $\mathcal{S}_q$ decay, as from Table II, are a heavy invisible particle manifesting as a MET, plus either an up-type quark or a down-type quark and a lepton-neutrino pair or quark-quark pair from the virtual $\mathcal{W}$ boson. While there are not yet dedicated analyses for this specific model at the LHC experiments, the considered production and decay modes share significant similarities with some SUSY scenarios. In particular, production via strong interaction of an $\mathcal{S}_q$ pair, and its decay to an invisible fermion plus a quark, shares several similarities with a pair production of squarks, which then further decay to quarks and neutralinos. We henceforth make use of results from the LHC that explore such signatures, in particular, Refs. [34,35].

For both the NMS and DMS, as at least y_Q^{33} and y_Q^{23} have to be different from zero, both top quarks plus MET and charm quarks plus MET final states need to be studied. The experimental signature for charm and up quarks at the LHC is not distinguishable at the moment, so they both manifest as a jet of hadrons in the detector. The observable quantities of interest in this case are the excluded cross sections for the top quark pair plus neutralino production, and the light quark pair plus neutralino production. It is important to recall that, for the chosen value of the hypercharge, the quantum numbers of the $\mathcal{S}_q$ boson are the same as the one of a (right-handed) stop quark, while the quantum numbers of $\mathcal{F}_L^\downarrow$ and $\mathcal{F}_L^\uparrow$ match those of Higgsinos, a neutralino and a chargino, respectively.

In order to constrain the production cross section of these processes, we perform the reinterpretation of two analyses studying in an exclusive way the production of quark pairs plus missing energy in the final state. In Refs. [34,35], limits on the cross section for $pp \to \tilde{t}\bar{t}^*$, with $\tilde{t} \to t\chi_0$ or $b\chi_+ \to b\mathcal{W}\chi_0$ are derived, where following the SUSY notation $\tilde{t}$ is the stop and $\chi_{0,+}$ are the neutralino and chargino, respectively. In Ref. [34], exclusion limits are set on $pp \to \tilde{q}\tilde{q}^* \to q\bar{q} + \chi_0\chi_0$, with q being a u, d, s, or c quark. The former limit can be used to put constraints on the $pp \to \mathcal{S}_q \mathcal{S}_q{}^*$, $\mathcal{S}_q \to t\mathcal{F}_L^\downarrow$ or $\mathcal{S}_q \to b\mathcal{F}_L^\uparrow$ production, and the latter for $pp \to \mathcal{S}_q \mathcal{S}_q{}^* \to c\bar{c} + \mathcal{F}_L^\downarrow \mathcal{F}_L^\downarrow$ or $pp \to \mathcal{S}_q \mathcal{S}_q{}^* \to u\bar{u} + \mathcal{F}_L^\downarrow \mathcal{F}_L^\downarrow$.

The inclusive cross sections via strong interaction for $pp \to \mathcal{S}_q \mathcal{S}_q{}^*$ are identical to the one for $pp \to \tilde{t}\bar{t}^*$ multiplied by the number of $\mathcal{S}_q$ scalars in the model, i.e., N_{TC}. In particular, the excluded cross section values are taken as a function of the mass of the stop (or light squark) and neutralino, and interpreted as excluded values of the cross section of an $\mathcal{S}_q$ and $\mathcal{F}_L^\downarrow$ with the same masses in the $\mathcal{F}_L^\downarrow + t(\mathcal{F}_L^\downarrow + c, \mathcal{F}_L^\downarrow + u)$ final state. In order to constrain the model, different values of N_{TC} as well as the coupling strengths and branching ratios are considered. The excluded cross sections, therefore, are evaluated as follows from the SUSY searches:

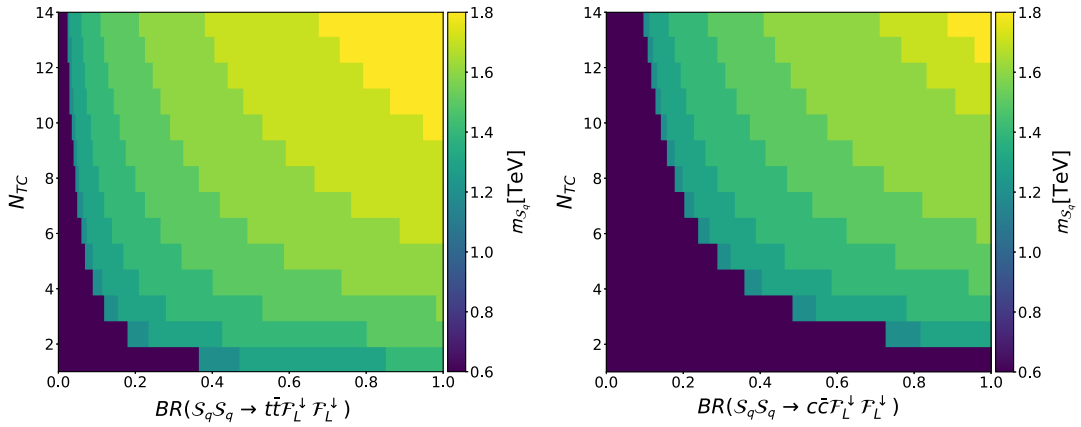

FIG. 5. Limits on the mass of the new $\mathcal{S}_q$ boson vs N_{TC} vs the branching ratio to $tt(cc) + \mathcal{F}_L^{\downarrow}\mathcal{F}_L^{\downarrow}$ in the $tt(cc)$ + invisible decay channel on the left (right).

$$\sigma(\mathcal{S}_q\mathcal{S}_q^*, \mathcal{S}_q \to t\mathcal{F}_L^{\downarrow} \quad \text{or} \quad \mathcal{S}_q \to b\mathcal{W}\mathcal{F}_{L0}^{\uparrow}) = \sigma(\tilde{t}\tilde{t}^*, \tilde{t} \to t\chi_0 \quad \text{or} \quad \tilde{t} \to b\mathcal{W}\chi_0) \times N_{TC}, \tag{15}$$

$$\sigma(\mathcal{S}_q\mathcal{S}_q^*) \times (\mathrm{BR}(c, \mathcal{F}_L^{\downarrow}) + \mathrm{BR}(u, \mathcal{F}_L^{\downarrow}))^2 = \sigma(\tilde{q}\tilde{q}^*, \tilde{q} \to \chi_0) \times N_{TC}. \tag{16}$$

We recall that $\mathrm{BR}(u, \mathcal{F}_L^{\downarrow})$ is negligible in the NMS, while it could be sizeable in the DMS.

The first results that can be extracted are the limits on the $\sigma(\mathcal{S}_q\mathcal{S}_q) \times \mathrm{BR}(t, \mathcal{F}_L^{\downarrow})^2$ and $\sigma(\mathcal{S}_q\mathcal{S}_q) \times \mathrm{BR}(c, \mathcal{F}_L^{\downarrow})^2$ reported in Fig. 5. By use of Eq. (8), it is possible to translate the upper limits on the branching ratio shown in Fig. 5 to a constraint on y_Q^{33}, y_Q^{32}, and y_Q^{31}. However, in order to extract constraints on the model, the flavor structure needs to be defined. Once $m_{\mathcal{S}_q}$ and $m_{\mathcal{F}_L^{\uparrow}}$ are set, Eqs. (A7), (A10), and (A13) allow us to identify a unique value of $(y_Q y_Q^{\dagger})_{bs}$. By exploiting the relations in Eqs. (13) and (14), it is possible to identify a range for y_Q^{33}, y_Q^{32}. If all are excluded, then the model for that combination of $m_{\mathcal{S}_q}$, $m_{\mathcal{F}}$, and N_{TC} is excluded. Figure 6, left, shows the limit on $(y_Q y_Q^{\dagger})_{bs}$ as a function of N_{TC} and $m_{\mathcal{S}_q}$, by keeping $m_{\mathcal{F}_L^{\downarrow}}$ fixed at 0.1 TeV. Finally, Fig. 6, right, shows the maximum value of $m_{\mathcal{F}_L^{\downarrow}}$ excluded as a function of N_{TC} and $m_{\mathcal{S}_q}$. Those values allow us to strongly constrain the model for values of $m_{\mathcal{S}_q}$ in the 0.7 TeV range, but only larger N_{TC} are excluded for values of $m_{\mathcal{S}_q}$ above 1 TeV.

C. Open channels

This reinterpretation can be extended by performing analyses in different directions:

(i) The analyses used as a benchmark do not include the potential case where the $\mathcal{S}_q$ pair decays to $tc + \mathcal{F}_L^{\downarrow}\mathcal{F}_L^{\downarrow}$. While this signature might be more challenging, this could help constrain the model further.

(ii) The $\mathcal{S}_q$ leg with one LLCP + b, s, or d quark is not considered. This could lead to challenging but

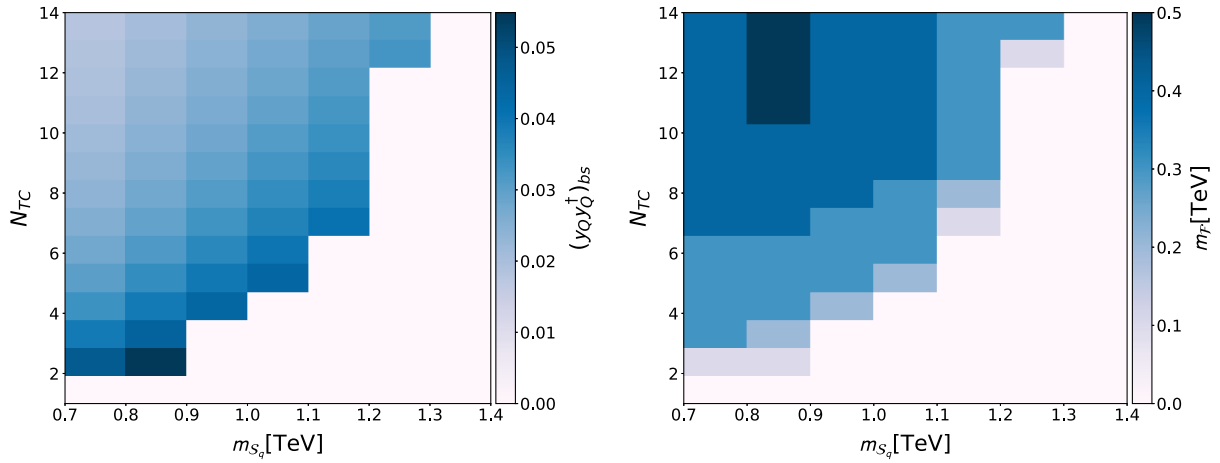

FIG. 6. Limits on the mass of the new $\mathcal{S}_q$ boson vs N_{TC} and vs the mixed coupling term $(y_Q y_Q^{\dagger})_{bs}$ (left, $m_{\mathcal{F}_L^{\downarrow}} = 0.1$ TeV), or vs the $m_{\mathcal{F}_L^{\downarrow}}$ (right).

well-identifiable final states with either two LLCP plus two quarks, or one LLCP plus one quark and a top or strange quark and MET.

(iii) No single production channel is considered. Further studies are needed to determine whether single production is relevant given the allowed coupling range.

(iv) Finally, this analysis only refers to the case $m_{\mathcal{S}_\ell} > \mathcal{F}_L^{\uparrow}$, $m_{\mathcal{S}_\ell} > \mathcal{F}_L^{\downarrow}$ in Table II, further channels are open to study.

V. SUMMARY AND RESULTS

The constraints from the LHC measurements can be used to derive information on the phase space available on $c_{b_L\mu_L}$ and Δa_μ by considering the relations in Eqs. (A5) and (A13) when excluding the values of $(y_Q y_Q^\dagger)_{bs}$ reported in the left panel of Fig. 6 and the values of $m_{\mathcal{S}_q}$ and $m_{\mathcal{F}_L^{\downarrow}}$ reported in the right panel of Fig. 6. The limits are evaluated for two different values of Δa_μ: First, only dispersive measurements from Refs. [6,36–56] are considered, then the entire analysis is repeated by taking into account the most recent values from lattice calculations as reported in Ref. [57], and results are reported in the following. The allowed values of $(y_Q y_Q^\dagger)_{bs}$ vs $(y_L y_L^\dagger)_{\mu\mu}$ before and after the application of LHC constraints for $N_{TC} = 9$ are reported in Fig. 7. Constraints on $c_{b_L\mu_L}$ and Δa_μ for a representative value of the coupling of $(y_Q y_Q^\dagger)_{bs} = 0.05$ are reported in Fig. 8. The black star illustrates the best fit for $c_{b_l\mu_L}$ and Δa_μ, and the darker and lighter purple bands represent the regions in agreement with the experimental values within 1 and 3 standard deviations, respectively.

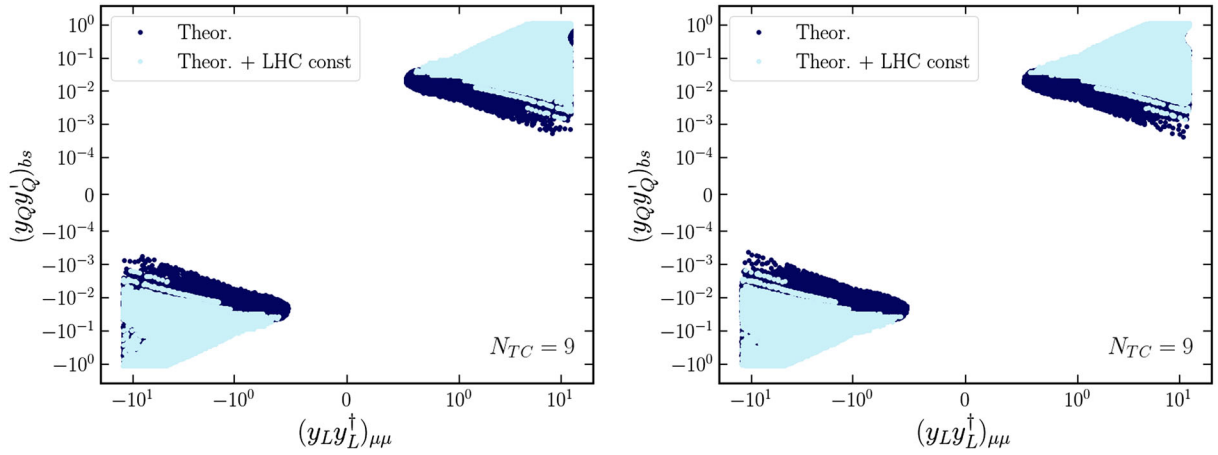

FIG. 7. Allowed values of $(y_Q y_Q^\dagger)_{bs}$ vs $(y_L y_L^\dagger)_{\mu\mu}$ before (dark blue) and after (azure) the application of constraints from the LHC. In the left plot, values of Δa_μ from dispersive measurements [6,36–56] are used, and in the right plot, lattice measurements [57] are used.

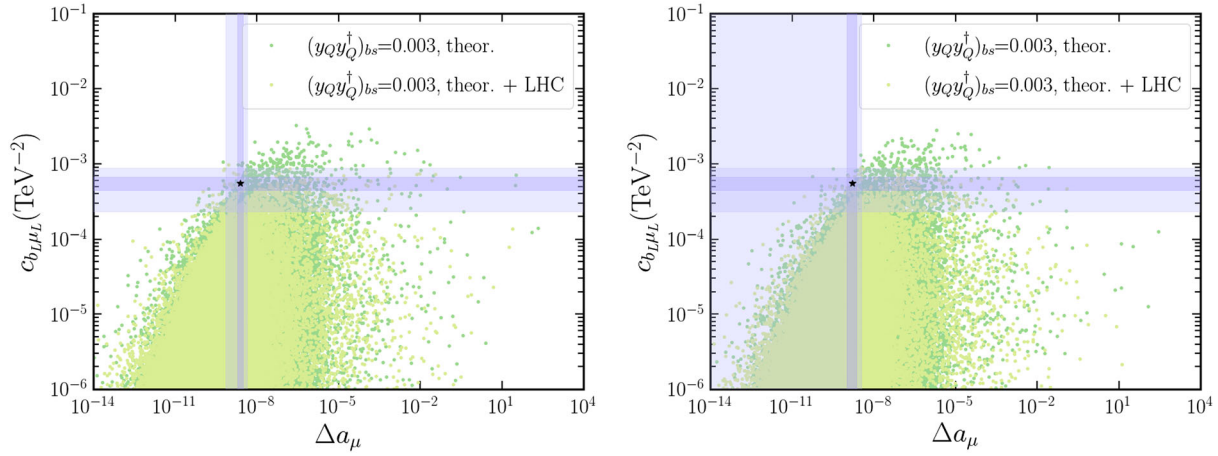

FIG. 8. Allowed values of $c_{b_L\mu_L}$ vs Δa_μ before (dark green) and after (bright green) the application of constraints from the LHC. In the left plot, values of Δa_μ from dispersive measurements [6,36–56] are used; in the right, plot lattice measurements [57] are used. The black stars indicate the best fit for $c_{b_L\mu_L}$ and Δa_μ; the dark and light violet lines depict the regions in agreement with the experimental values within 1 and 3 standard deviations, respectively.

The constraints obtained hold true for the cases where $|m_{\mathcal{F}_L^\uparrow} - m_{\mathcal{F}_L^\downarrow}| < m_{\mathcal{W}}$ and $m_{SE} > m_{\mathcal{F}_L^\uparrow}, m_{\mathcal{F}_L^\downarrow}$. In other scenarios reported in Sec. III, such results only partially constrain the model, as there is freedom for the $\mathcal{S}_q$ boson to decay through different decay chains with respect to the ones considered in Sec. IV. Dedicated analyses on proton-proton collision data, searching for LLCPs, or MET plus quarks and leptons, as described in Table II, would allow us to detect the model's signals for not-yet-excluded scenarios. Even in the absence of a signal, an analysis similar to the one presented in Sec. III can be applied to further constrain the model.

VI. CONCLUSIONS

For the past decades, several extensions of the SM have been put forward ranging from the time-honored minimal supersymmetric version to composite and radiative realizations including extra dimensions. At the same time, evidence is being accumulated experimentally indicating the existence of new physics beyond the SM. The goal of this work is to establish a phenomenological template mimicking different models from radiative to composite, depending on how the underlying dynamics is realized, and show that it can also be adopted as an experimental template of new physics by either suggesting new searches or adapting earlier ones to either discover or constrain the parameter space of the theory. Another crucial aspect is that the model is sufficiently flexible to accommodate the various observed SM anomalies.

Specifically, as a first step, we consider a radiative extension of the SM that reconciles the various experimental results while further predicting the existence of new bosons and fermions with a mass spectrum in the TeV energy scale. The resulting spectrum is, therefore, within the reach of the LHC experiments. We suggest new interesting search strategies including the associate production of SM particles with invisible or long-lived charged particles. We further show that it is possible to employ earlier SUSY-inspired searches to constrain the spectrum and couplings of the newly introduced particles. We also check that the template is sufficiently rich to accommodate the observed experimental anomalies while allowing for new experimental signatures at the LHC.

ACKNOWLEDGMENTS

R. C. and S. M.'s work was supported by the research Grant No. 2017W4HA7S "NAT-NET: Neutrino and Astroparticle Theory Network" under the program PRIN 2017 funded by the Italian Ministero dell'Università e della Ricerca and by the research project Theoretical Astroparticle Physics funded by the Istituto Nazionale di Fisica Nucleare. G. C. is grateful to the LABEX Lyon Institute of Origins (Grant No. ANR-10-LABX-0066) Lyon for its financial support within the program "Investissements d'Avenir" of the French government operated by the National Research Agency.

APPENDIX A: ANOMALIES AND HIGH-PRECISION MEASUREMENT CONSTRAINTS

In this section, we list and review all the precision measurements that significantly constrain the radiative model. Besides the muon anomalies in $R_{K^{(*)}}$ and $g-2$, we consider modifications of the Higgs coupling to muons, $B_0 - \bar{B}_0$ mass mixing, and the recent discrepancy in the $\mathcal{W}$ boson mass measurement at CDF II. In each subsection, we report how the radiative model affects the theoretical estimation of each observable. In the last subsection, we comment how mass splits in the new fermions could explain the $\mathcal{W}$ boson mass value. The impact of these bounds on collider searches will be discussed in the following section.

1. Radiative muon mass and the Higgs coupling

The new Yukawa interactions in Eq. (1) contribute at one-loop level to all SM fermion masses, in addition to the SM-like Yukawa couplings. In fact, all masses could be generated radiatively, except for the top quark one, whose Yukawa coupling is of order one. In a general setup, cancellations may occur between the tree-level coupling and the loops; hence, one could have sizeable modifications of the Higgs coupling to the fermions.

As we are interested in anomalies in the muon sector, below we illustrate this effect for the muon. Schematically, ignoring lepton flavor mixing terms, the muon mass will be given by two competing terms:

$$m_\mu = \frac{y_\mu^{\rm SM} v}{\sqrt{2}} + \delta m_\mu^{\rm loop},$$
$$\delta m_\mu^{\rm loop} = N_{TC} \frac{(y_L y_E)_{\mu\mu}}{16\pi^2} \frac{k_\uparrow v}{\sqrt{2}} F_{\rm loop}(\text{masses}), \quad \text{(A1)}$$

where $F_{\rm loop}$ is an order one function of the mass parameters [30], and m_μ is the measured muon mass. The physical coupling of the Higgs boson to muons also receives a correction with respect to the SM value given schematically by

$$y_\mu^{\rm eff} = y_\mu^{\rm SM}\left(1 + \frac{\delta m_\mu^{\rm loop}}{m_\mu} k_\uparrow^2 G_{\rm loop}(\text{masses})\right), \quad y_\mu^{\rm SM} = \frac{\sqrt{2} m_\mu}{v}, \quad \text{(A2)}$$

where the function $G_{\rm loop}$ depends on the mass parameters. Evidence for this coupling has been recently obtained at the LHC Run-2 by the ATLAS and CMS Collaborations [58,59]: Current data are consistent with the SM value at the 43% level, while projections for the full run of the LHC indicate that precision below 5% is achievable [60].

Hence, the correction encoded in the second term in the parentheses of Eq. (A2), proportional to $\delta m_\mu^{\rm loop}$, must be smaller than unity in absolute value.

If we allow for cancellations between the two terms in Eq. (A1), large muon couplings to the new fermions and scalars could generate $\delta m_\mu^{\rm loop} \gg m_\mu$, hence, dangerously enhancing the correction to the muon Higgs coupling. There are two ways out: The coupling $k_\uparrow$ could be small, however suppressing the radiatively induced SM fermion masses to be of the order of the muon mass for all down-type fermions, or we could ask the product $(y_L y_E)_{\mu\mu}$ to be small for muons. Sizeable effects in muon physics are preserved if y_L is sizeable while y_E is small, as also preferred by R_K (as we will see below). In this work, we will follow the latter possibility. In summary, as long as $(y_L y_E)_{\mu\mu} \sim m_\mu/v$ via a small y_E, the correction to the Higgs coupling to muons is under control without affecting the observables in the muon anomalies.

2. R_K and R_{K^*} anomalies

The relevant effective Hamiltonian for $B \to K^{(*)} ll$ transitions is given by the following operators [22]:

$$\mathcal{H}^{\rm eff} = -\frac{\alpha}{4\pi}\frac{4G_F}{\sqrt{2}} V_{tb}V_{ts}^* C_L^{ij}\mathcal{O}_L^{ij}, \tag{A3}$$

where

$$\mathcal{O}_L^{ij} = [\bar{s}\gamma^\mu P_L b][\bar{l}^i\gamma_\mu(1-\gamma_5)l^j] \equiv \mathcal{O}_9^{ij} - \mathcal{O}_{10}^{ij}. \tag{A4}$$

We recall that the operator with right-handed quarks is absent in the SM, and it is disfavored as a NP origin of the anomaly by data; hence, we will not consider it here. The dimensionful Wilson coefficients are

$$c_{b_L\mu_L} = -\frac{\alpha}{4\pi}\frac{4G_F}{\sqrt{2}} V_{tb}V_{ts}^*, \qquad c_L^{\mu\mu} = -\frac{C_L^{\mu\mu}}{(36\ \text{TeV})^2} \tag{A5}$$

that encode NP contributions in the muon final state. More details on the effective Hamiltonian and notation for the coefficients are reviewed in [12]. It is possible to rewrite the R_K ratio as follows:

$$R_K = \frac{|C_L^{\rm SM} + \Delta C_L^{\mu\mu}|^2}{|C_L^{\rm SM}|^2}, \tag{A6}$$

where $C_L^{\rm SM} \approx 8.64$ (and we neglect the much smaller contribution to right-handed leptons) [61] is the same for muons and electrons. For R_{K^*}, a similar expression holds. The one-loop diagrams stemming from the radiative model in Eq. (1) are reported in Fig. 9. As we assume $y_L \gg y_E$ for the muons, the relevant contributions are the one with left-handed quarks. In Ref. [61] is reported the expression for the Wilson coefficient for the model being examined:

$$c_{b_L\mu_L} = N_{TC}\frac{(y_L y_L^\dagger)_{\mu\mu}(y_Q y_Q^\dagger)_{bs}}{(4\pi)^2 m^2_{\mathcal{F}_{L\uparrow}}}\frac{1}{4}F(x,y), \tag{A7}$$

where $x = m^2_{\mathcal{S}_q}/m^2_{\mathcal{F}_{L\uparrow}}$, $y = m^2_{\mathcal{S}_\ell}/m^2_{\mathcal{F}_{L\uparrow}}$, and the loop functions expression is reported in Appendix C. Note that we have neglected the mixing between the fermions $\mathcal{F}$ induced by the $k_\uparrow$ coupling in Eq. (1).

To extract bounds on the model parameter space, we impose the latest LHCb result, combining Runs 1 and 2 data given by [8]

$$R_K|_{\rm exp} = 0.846^{+0.042}_{-0.039}(\text{stat})^{+0.013}_{-0.012}(\text{syst}) \tag{A8}$$

in the $q^2 = [1.1, 6]\ \text{GeV}^2$ window. In practice, we require $0.807 < R_K < 0.888$ [12]. Note that R_{K^*} leads to similar bounds, and we do not include it for simplicity.

In [12], the reader can find an in-depth model-independent study of these anomalies.

3. $B_0 - \bar{B}_0$ mass mixing

The contributions to the $B_0 - \bar{B}_0$ mass mixing arise from the diagrams at one-loop level shown in Fig. 10. The dominant contributions are associated with the diagrams with left-handed quarks. These contributions can be written in terms of the following effective Hamiltonian [22]:

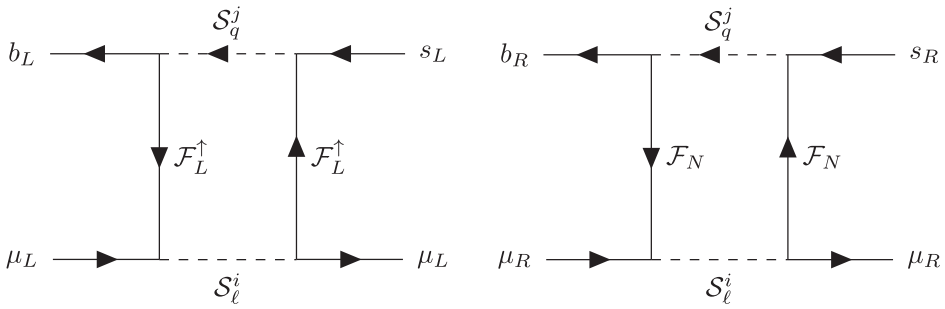

FIG. 9. Radiative contribution to the $B \to K ll$ transition that affects R_K. In the right (left) panel is shown the contribution due to right- (left-) handed quarks. The diagram that is used to compute the quantity $c_{b_L\mu_L}$ is the one on the left as $y_E \ll y_L$.

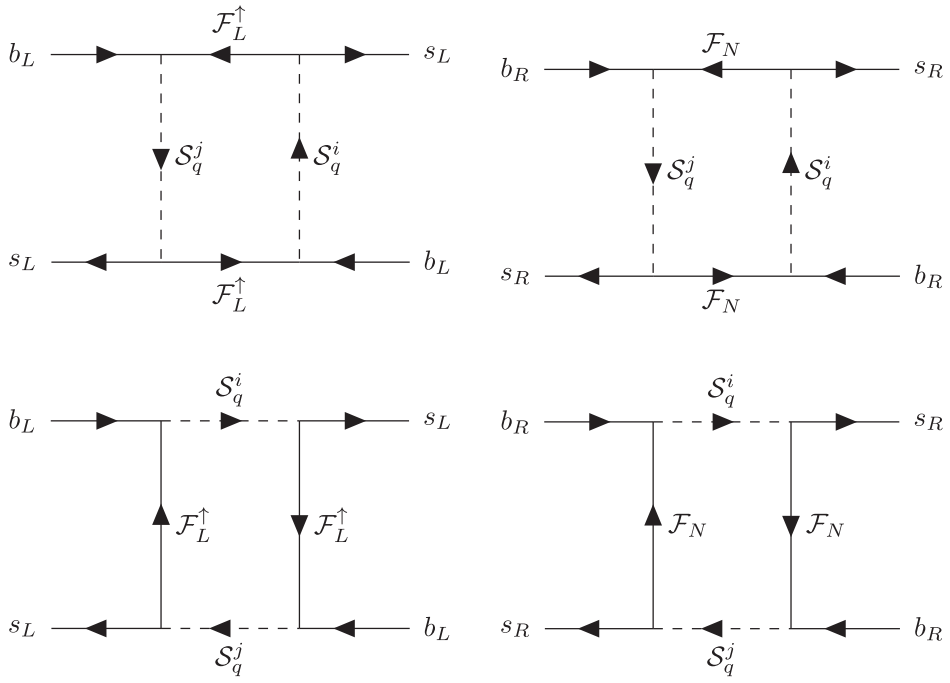

FIG. 10. Radiative contribution to the B – $\bar{\text{B}}$ mixing. In the left (right) panel are shown the contributions with left- (right-) handed quarks. As for R_K, the dominant contribution comes from the operators with left-handed quarks.

$$\mathcal{H}_{\text{eff}}^{B\bar{B}} = C_{B\bar{B}}[\bar{s}_\alpha \gamma^\mu P_L b_\alpha][\bar{s}_\beta \gamma_\mu P_L b_\beta], \tag{A9}$$

where α and β are color indices. The NP contribution from the radiative model under investigation is given by [61]

$$C_{B\bar{B}}^{\text{NP}} = N_{TC}\frac{(y_Q y_Q^\dagger)_{bs}^2}{(4\pi)^2 m_{\mathcal{F}_L^\uparrow}^2}\frac{1}{8}F(x,x), \tag{A10}$$

where the loop function is defined in Appendix C and $x = m_{\mathcal{S}_q}^2/m_{\mathcal{F}_L^\uparrow}^2$. It is possible to obtain constraints on the Wilson coefficient $C_{B\bar{B}}$ in terms of the ratio [22]

$$R_{\Delta B_s} = \frac{\Delta M_{B_s}^{\text{exp}}}{\Delta M_{B_s}^{\text{SM}}} - 1 = \frac{C_{B\bar{B}}^{\text{NP}}}{C_{B\bar{B}}^{\text{SM}}}, \tag{A11}$$

where the SM prediction is $C_{B\bar{B}}^{\text{SM}}(2M_W) \simeq 8.2 \times 10^{-5}$ TeV^{-2} and the current bound on the NP contribution reads $C_{B\bar{B}}^{\text{NP}} \in [-2.8, 1.3] \times 10^{-5}$ TeV^{-2} [22] at 3 standard deviations.

4. Muon $g-2$ anomaly

The new fermions and scalars contribute to the anomalous magnetic moment of the muon via their left-handed couplings y_L, as shown by the left graph in Fig. 11. Additionally, the model contains a contribution proportional to the Yukawa coupling $k_\uparrow$, as shown by the representative diagram in the right panel of Fig. 11. This term will be proportional to the product of Yukawas $(y_L y_E)_{\mu\mu} k_\uparrow$, which also contributes to the muon mass, as shown in Eq. (A1). The NP contribution can be computed in terms of the following operator [22]:

$$\mathcal{H}_{\text{eff}}^{a_\mu} = -a_\mu \frac{e}{4m_\mu}[\bar{\mu}\sigma^{\mu\nu}\mu]F_{\mu\nu}, \tag{A12}$$

where m_μ is the muon mass and e is the electron charge. The NP contribution to a_μ is given by [61]

$$\Delta a_\mu = \frac{N_{TC} m_\mu^2}{(4\pi)^2 m_{\mathcal{F}_L^\uparrow}^2}\left(\frac{(y_L y_E)_{\mu\mu} k_\uparrow v}{m_\mu}[2q_{\mathcal{S}_E}F_{LR}(y) + 2q_{\mathcal{F}}G_{LR}(y)] + (y_L y_L^\dagger)_{\mu\mu}\left[2q_{\mathcal{S}_E}F_7(y) + 2q_{\mathcal{F}}\tilde{F}_7(y)\right]\right), \tag{A13}$$

where $x = m_{\mathcal{S}_q}^2/m_{\mathcal{F}_L^\uparrow}^2$ and $y = m_{\mathcal{S}_\ell}^2/m_{\mathcal{F}_L^\uparrow}^2$. Here, $q_{\mathcal{F}}$ and $q_{\mathcal{S}_E}$ are the charges of $\mathcal{F}_L^\uparrow$ ($q_{\mathcal{F}} = -1$) and $\mathcal{S}_\ell$ ($q_{\mathcal{S}_E} = 0$), respectively. In our case, we have only the contribution from $\mathcal{F}_L^\uparrow$ since $\mathcal{S}_\ell$ is neutral. The loop functions are reported in Appendix C.

The main uncertainty on the SM prediction for a_μ comes from the hadronic contribution to the photon vacuum polarization. Recent lattice results [57,62–64] are in tension with data-driven approaches based on dispersion relations [40–45,65]. In the numerical analysis, we consider NP contributions in agreement with the lattice results [57] $\Delta a_\mu = (165 \pm 60) \times 10^{-11}$ or dispersion estimates $\Delta a_\mu = (251 \pm 59) \times 10^{-11}$ [6].

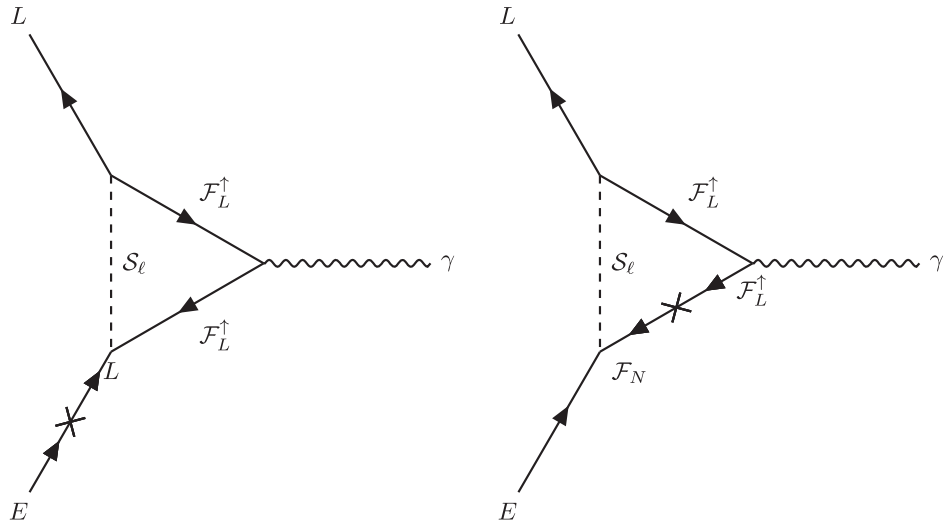

FIG. 11. One-loop contributions to $(g-2)_\mu$ from the radiative model under investigation.

5. $M_{\mathcal{W}}$ anomaly

Recently, the CDF II Collaboration at the Fermilab Tevatron Collider reported a new estimation of the $\mathcal{W}$ boson mass using a sample of approximately (4×10^6) $\mathcal{W}$ bosons. In Ref. [66], it is reported that

$$M_{\mathcal{W}}^{\mathrm{CDF}} = 80433.5 \pm 6.4_{\mathrm{stat}} \pm 6.9_{\mathrm{syst}} = 80433.5 \pm 9.4 \text{ MeV}. \tag{A14}$$

The theoretical prediction for the same quantity within the SM, as reported in Ref. [67], is

$$M_{\mathcal{W}}^{\mathrm{th}} = 80357 \pm 4_{\mathrm{inputs}} \pm 4_{\mathrm{theory}} \text{ MeV}. \tag{A15}$$

The theoretical estimation is obtained with a combination of perturbative expansions and a set of high-precision measurements of observables in the EW sector. The uncertainty on such a quantity can be divided into two components. One is related to the uncertainties of the observables used, and the latter is related to higher-order terms in the perturbative SM calculation. It can be easily shown that

$$\Delta M_{\mathcal{W}}|_{\mathrm{CDF}} = M_{\mathcal{W}}^{\mathrm{CDF}} - M_{\mathcal{W}}^{\mathrm{th}} = 76 \pm 11 \text{ MeV}. \tag{A16}$$

This means that there is a 7 standard deviation discrepancy between the CDF experimental measurement and the theoretical estimation. Previous measurements summarized in Table IV have a smaller accuracy and central values closer to the SM prediction. A weighted average should be considered, however, with error increased by the $\sqrt{\chi^2/\mathrm{ndf}}$ factor [67] to account for the large discrepancies among the four measures. The result determined in [12] yields

$$M_W^{\mathrm{AVG}} = 80409 \pm 17 \text{ MeV}. \tag{A17}$$

The deviation from the SM reduces to around 3 standard deviations:

$$\Delta M_{\mathcal{W}}|_{\mathrm{AVG}} = M_{\mathcal{W}}^{\mathrm{AVG}} - M_{\mathcal{W}}^{\mathrm{th}} = 52 \pm 18 \text{ MeV}. \tag{A18}$$

It is possible to explain Eqs. (A14) or (A17) by introducing beyond the SM physics as summarized in [12]. The corrections from NP to the $\mathcal{W}$ boson mass can be expressed via the following approximate formula [71]:

$$\Delta M_{\mathcal{W}}^{\mathrm{NP}} \approx 300 \text{ MeV}(1.43\,T - 0.86\,S), \tag{A19}$$

where T and S are the so-called EW oblique parameters [72–74]. We use the definition of S and T shown in Ref. [75] reported in the following:

TABLE IV. Recent measurements of the $\mathcal{W}$ boson mass at colliders.

	LEP + TeVatron [68]	ATLAS [69]	LHCb [70]	CDF-II [66]
Measurement	80385 ± 15 MeV	80370 ± 19 MeV	80354 ± 32 MeV	80433.5 ± 9.4 MeV
Pull from SM	28 ± 16 MeV	13 ± 19 MeV	-3 ± 32 MeV	76 ± 11 MeV

$$S = -16\pi \frac{\Pi_{3Y}(M_Z^2) - \Pi_{3Y}(0)}{M_Z^2},$$
$$T = 4\pi \frac{\Pi_{11}(0) - \Pi_{33}(0)}{s_W^2 c_W^2 M_Z^2}, \tag{A20}$$

where $s_W = \sin\theta_W$ and $c_W = \cos\theta_W$, θ_W being the Weinberg angle defined at the scale $\mu = M_Z$, Π_{3Y} is the vacuum polarization of one ispospin and one hypercharge current, while Π_{11} and Π_{33} are the vacuum polarization of the isospin currents. We illustrate the impact of the $\mathcal{W}$ boson mass measurement on EW physics in Fig. 12, where a red star indicates the SM prediction at one-loop level, which corresponds to $T = S = 0$. The black dot marks the observed value for the oblique parameters without including the CDF result, corresponding to $T = 0.09 \pm 0.14$, $S = 0.04 \pm 0.11$, with a covariance of $\rho = 0.92$ [76]. The dashed orange ellipse and the shaded orange ellipse correspond, respectively, to the covariance ellipse drawn at 1σ and 3σ of the oblique parameters measure. They include several EW precision measurements, including the $\mathcal{W}$ boson mass: To separate its impact, we show the determination of T and S from separate sources. The light yellow dashed lines and the yellow region correspond to the bound originating from asymmetries measured at LEP experiments and from the determination of $\sin^2\theta_W^{\rm eff}$. The pink dashed line and the pink region is driven by the CDF mass measurement $M_{\mathcal{W}}|_{\rm CDF}$ within 1σ and 3σ, respectively. The same reasoning applies to the light violet dashed lines and light violet region, which are relative to the average estimation $M_{\mathcal{W}}|_{\rm AVG}$. We remark that the new measurement pushes the preferred region toward positive values of T with respect to the SM and the old results. This is confirmed by new EW fits that include the CDF result in the average [14,15] or in replace of the old values [16]. Hence, the new physics effect must be related to some breaking of the custodial symmetry defined in the SM Higgs sector.

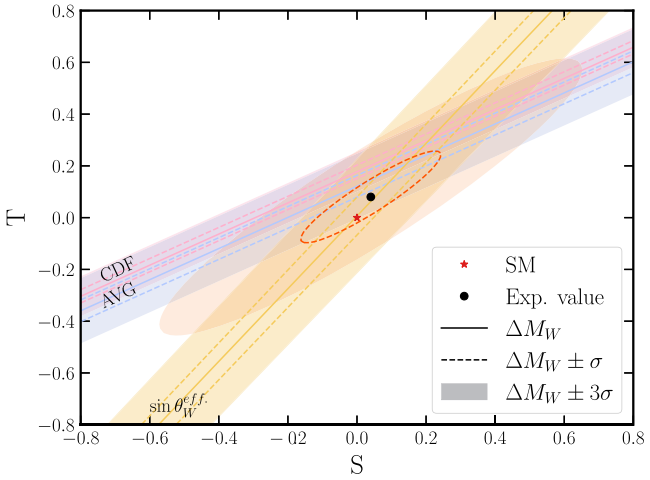

FIG. 12. In pink (violet) is shown the parameter space region that is able to explain the $\Delta M_{\mathcal{W}}|_{\rm CDF}$ ($\Delta M_{\mathcal{W}}|_{\rm AVG}$) within 3σ. The black dot represents the experimental value of T and S, and the orange ellipse is the corresponding covariance ellipse at 3σ. The yellow region represents the bound originating from asymmetries and determination of $\sin^2\theta_W^{\rm eff}$.

In the radiative model under investigation, this effect may dominantly arise from a mass difference between the components of the doublet of fermions $\mathcal{F}_L^{\uparrow}$ and $\mathcal{F}_L^{\downarrow}$, which contribute at one-loop level to the $\mathcal{W}$ boson mass. In Fig. 13, we show the relevant diagram for this correction. This effect can be expressed in terms of the oblique parameters in Eq. (A20), which take the following expressions:

$$S = \frac{N_{TC}}{6\pi}\left\{2(4Y+3)x_1 + 2(-4Y+3)x_2 - 2Y\ln\frac{x_1}{x_2} + \left[\left(\frac{3}{2}+2Y\right)x_1 + Y\right]g(x_1) + \left[\left(\frac{3}{2}-2Y\right)x_2 - Y\right]g(x_2)\right\},$$
$$T = \frac{N_{TC}}{8\pi s_W^2 c_W^2} f(x_1, x_2), \tag{A21}$$

where $x_1 = (m_{\mathcal{F}_L^{\uparrow}}/M_Z)^2$, $x_2 = (m_{\mathcal{F}_L^{\downarrow}}/M_Z)^2$, and

$$f(x_1,x_2) = \frac{x_1+x_2}{2} - \frac{x_1 x_2}{x_1 - x_2}\ln\frac{x_1}{x_2},$$
$$g(x) = -4\sqrt{4x-1}\arctan\frac{1}{\sqrt{4x-1}}. \tag{A22}$$

For equal masses $x_1 = x_2$, the contribution to T vanishes as $f(x,x) = 0$. This is clearly understood as such a mass difference can only occur via breaking of the weak isospin, which is generated by the mixing induced by the couplings

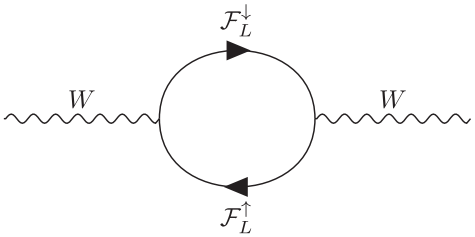

FIG. 13. Loop correction to $\mathcal{W}$ boson mass stemming from the radiative model.

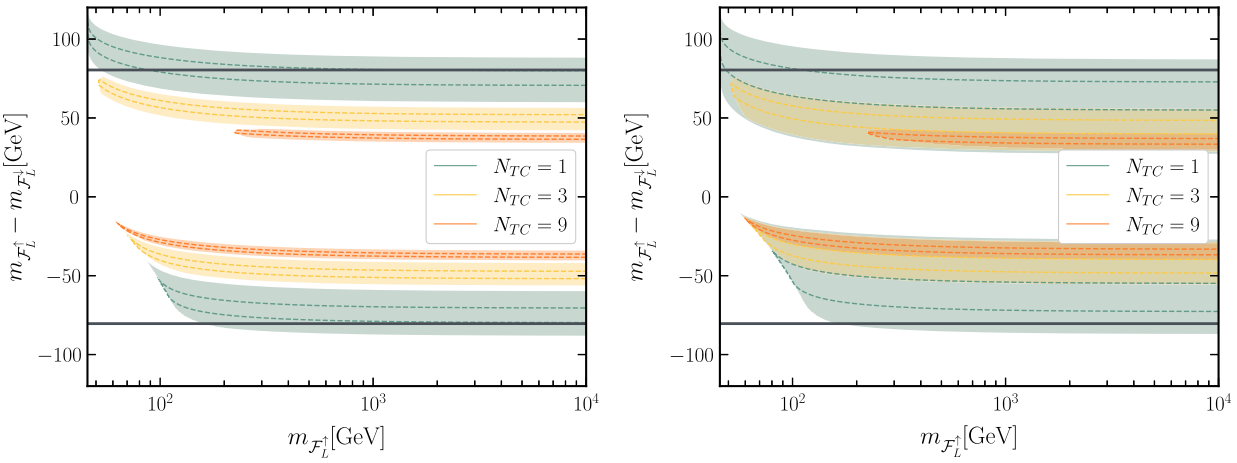

FIG. 14. In color is shown the parameter space that is able to compensate $\Delta M_{\mathcal{W}}$ from CDF II (left panel) and the average value shown in Eq. (A18) (right panel). For each N_{TC}, the bands represent the 3σ allowed region, while the dashed lines show the 1σ contour.

$k_\uparrow \neq k_\downarrow$. Hence, the states running in the loop should be the final mass eigenstates after diagonalization. The results in Eq. (A21) are valid in the limit of small mixing.

In Fig. 14 on the left (right) panel, we show the parameter space region that is able to explain $\Delta M_{\mathcal{W}}|_{\rm CDF}$ ($\Delta M_{\mathcal{W}}|_{\rm AVG}$) within 3σ for fixed values of N_{TC}, corresponding to different color shading. The dashed lines represent the agreement within 1σ with the experimental measurements. The plot investigates the dependence on the $\mathcal{F}_L$ mass versus the mass difference: The horizontal lines correspond to mass splits equal to $M_{\mathcal{W}}$ reported as a reference. In the region above (below) the top (bottom) line, decays among the two components are kinematically open, hence allowing the on-shell decay

$$\mathcal{F}_L{}^\uparrow \to \mathcal{W}^- + \mathcal{F}_L{}^\downarrow (\mathcal{F}_L{}^\downarrow \to \mathcal{W}^+ + \mathcal{F}_L{}^\uparrow). \tag{A23}$$

The plots show that, for $N_{TC} > 1$, the mass splits are required to be smaller than the W mass, but still sizeable. Henceforth, the above decays can still occur via an off-shell $\mathcal{W}$ boson.

If the isospin breaking in the fermion sector is too small, the leading effect may arise at two-loop level, involving the couplings y_Q^{ij} with the third-generation quarks. The mass difference between top and bottom already induces a sizeable isospin violation, while the loop suppression can be compensated by the large y_Q couplings of the third-generation quarks.

APPENDIX B: PARAMETER SPACE

Figures 15 and 16 show the available parameter space, respectively, using the dispersive [6,36–56] and lattice [57] Δa_μ measurements, in the planes $(y_Q y_Q^\dagger)_{bs}$ vs $(y_L y_L^\dagger)_{\mu\mu}$, $(y_L y_E^\dagger)_{\mu\mu^\kappa}$ vs $(y_Q y_Q^\dagger)_{bs}$, and $(y_L y_E^\dagger)_{\mu\mu^\kappa}$ vs $(y_L y_L^\dagger)_{\mu\mu}$.

APPENDIX C: LOOP FUNCTIONS

In this section, we report the loop functions used in Appendix A:

$$\begin{aligned}
F(x,y) &= \frac{1}{(1-x)(1-y)} + \frac{x^2 \ln x}{(1-x)^2(x-y)} \\
&\quad + \frac{y^2 \ln y}{(1-y)^2(y-x)}, \\
F(x,1) &= F(1,x) = \frac{-1+4x-3x^2+2x^2\ln x}{2(-1+x)^3}, \\
F(x,x) &= \frac{1-x^2+x\ln x}{(1-x)^3}, \\
F(1,1) &= \frac{1}{3},
\end{aligned} \tag{C1}$$

$$\begin{aligned}
\tilde{F}_7(y) &= \frac{F_7(y^{-1})}{y} = \frac{1-6y+3y^2+2y^3+6y^2\ln y}{12(1-y)^4}, \\
\tilde{F}_7(1) &= \frac{1}{24},
\end{aligned} \tag{C2}$$

$$\begin{aligned}
G_{LR}(y) &= \frac{1-4y+3y^2-2y^2\ln y}{2(1-y)^3}, \\
G_{LR}(1) &= \frac{1}{3},
\end{aligned} \tag{C3}$$

$$\begin{aligned}
F_{LR}(y) &= 1, \\
F_{LR}(1) &= \frac{1}{6}.
\end{aligned} \tag{C4}$$

Such functions were taken from [22,23] and adapted to our case.

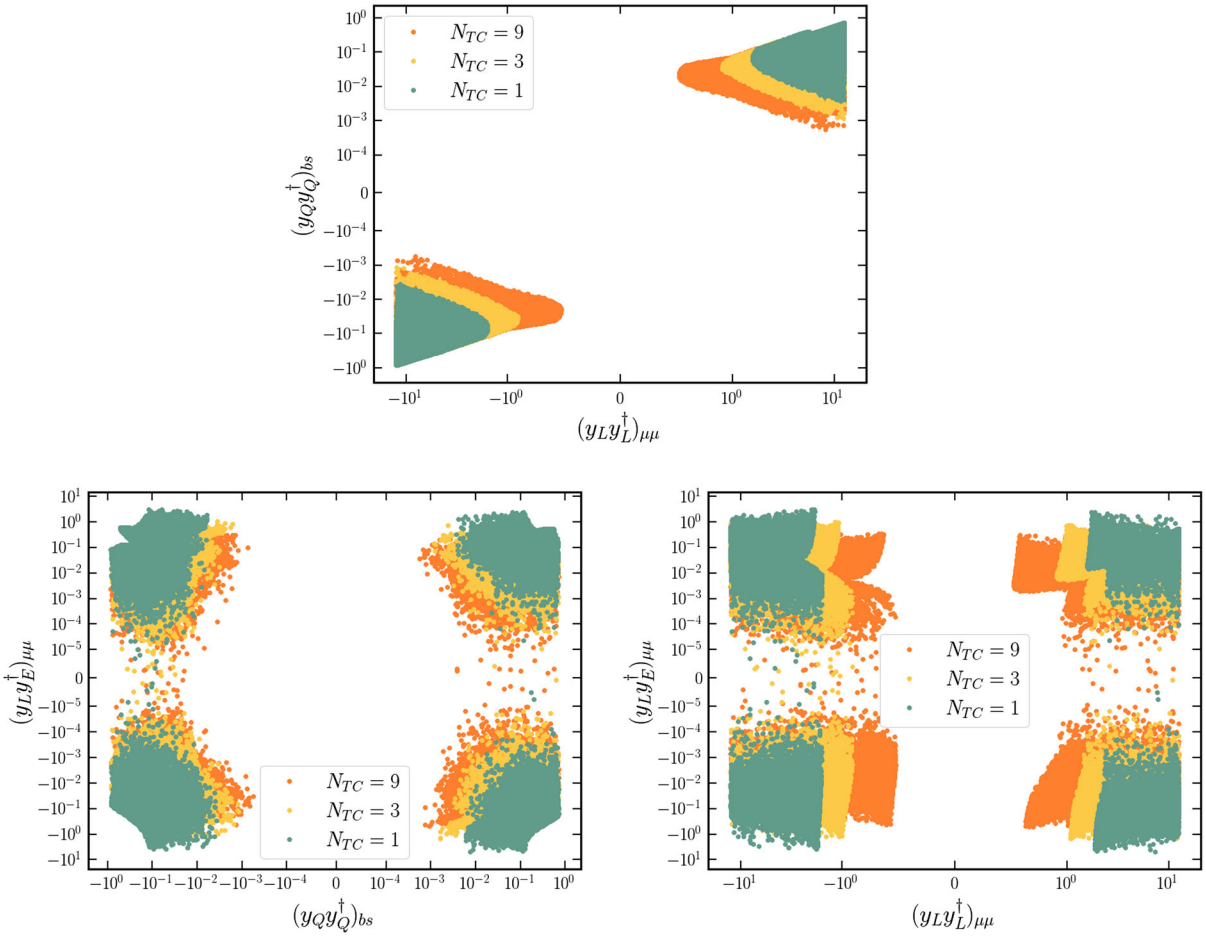

FIG. 15. Parameter space for $(y_Q y_Q^\dagger)_{bs}$ vs $(y_L y_L^\dagger)_{\mu\mu}$ (top), $(y_L y_E^\dagger)_{\mu\mu^K}$ vs $(y_Q y_Q^\dagger)_{bs}$ (bottom left), and $(y_L y_E^\dagger)_{\mu\mu^K}$ vs $(y_L y_L^\dagger)_{\mu\mu}$ (bottom right) using the dispersive Δa_μ measurement [6,36–56].

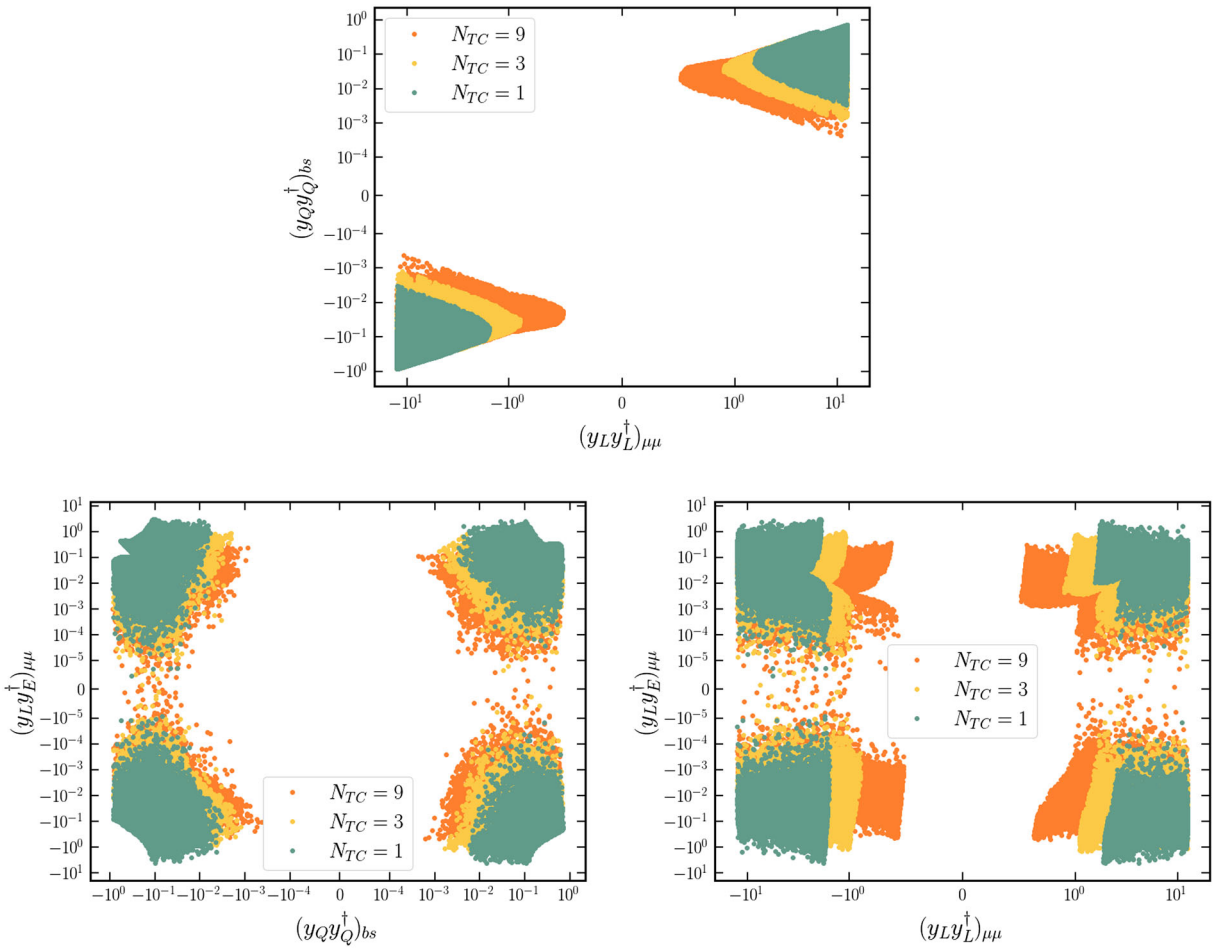

FIG. 16. Parameter space for $(y_Q y_Q^\dagger)_{bs}$ vs $(y_L y_L^\dagger)_{\mu\mu}$ (top), $(y_L y_E^\dagger)_{\mu\mu^K}$ vs $(y_Q y_Q^\dagger)_{bs}$ (bottom left), and $(y_L y_E^\dagger)_{\mu\mu^K}$ vs $(y_L y_L^\dagger)_{\mu\mu}$ (bottom right) using the lattice Δa_μ measurement [57].

APPENDIX D: DIAGRAMS

1. Single $\mathcal{S}_q$

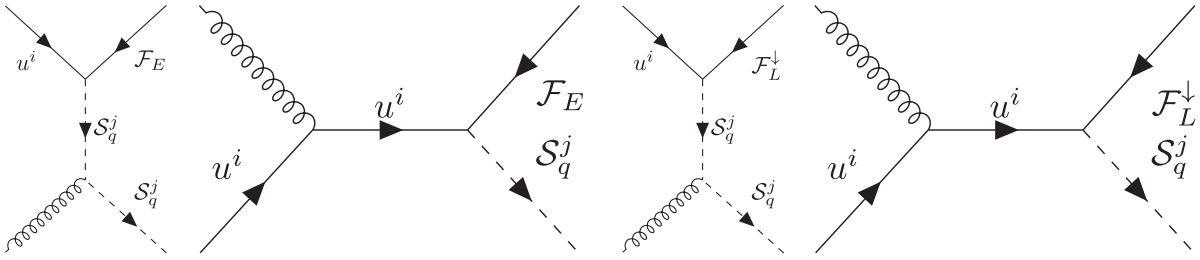

2. Double $\mathcal{F}$

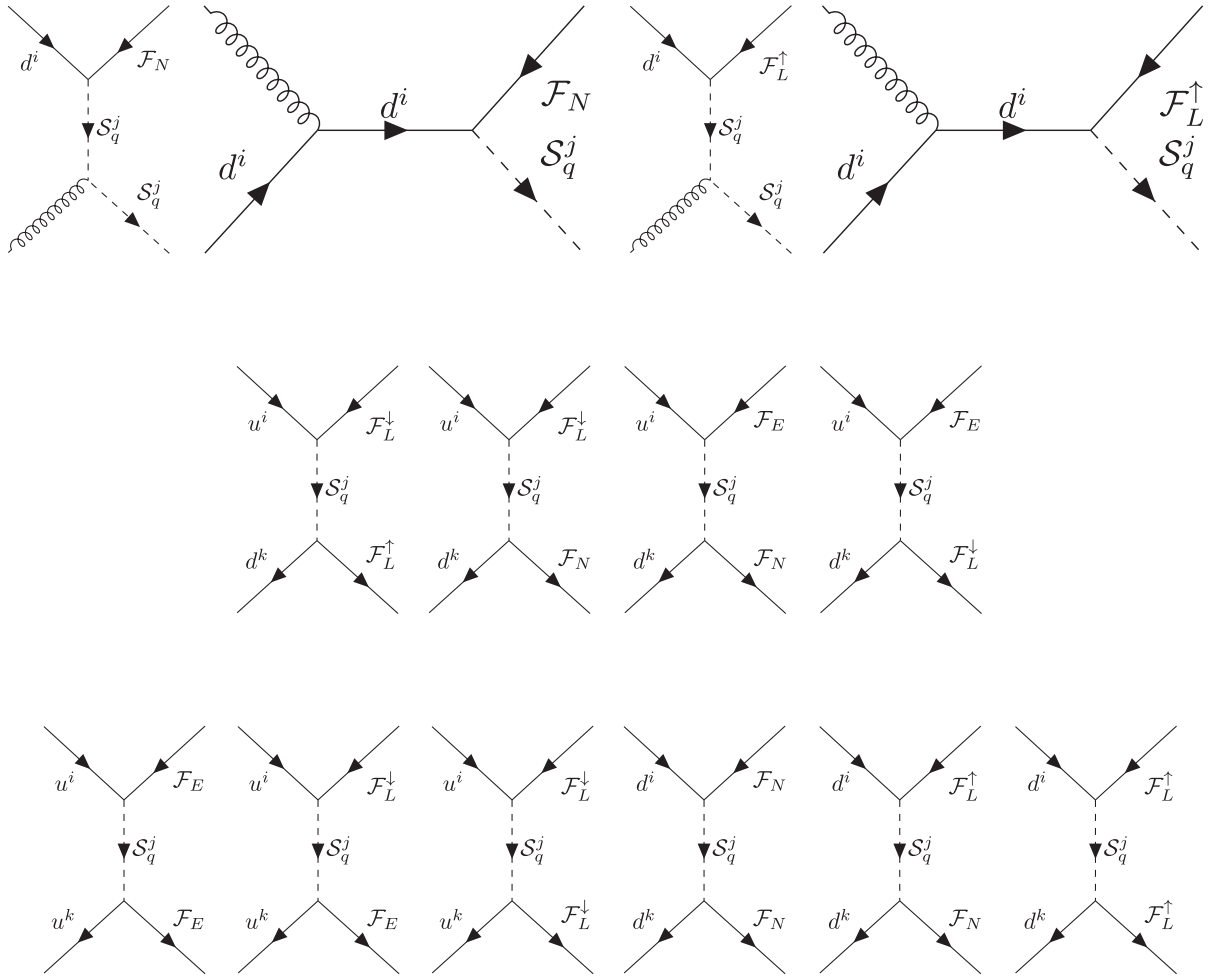

[1] G. W. Bennett *et al.* (Muon $g-2$ Collaboration), Final report of the E821 muon anomalous magnetic moment measurement at BNL, Phys. Rev. D **73**, 072003 (2006).

[2] J. P. Lees *et al.* (*BABAR* Collaboration), Evidence for an Excess of $\bar{B} \to D^{(*)}\tau^-\bar{\nu}_\tau$ Decays, Phys. Rev. Lett. **109**, 101802 (2012).

[3] S. Hirose *et al.* (Belle Collaboration), Measurement of the τ Lepton Polarization and $R(D^*)$ in the Decay $\bar{B} \to D^*\tau^-\bar{\nu}_\tau$, Phys. Rev. Lett. **118**, 211801 (2017).

[4] R. Aaij *et al.* (LHCb Collaboration), Measurement of the Ratio of Branching Fractions $\mathcal{B}(\bar{B}^0 \to D^{*+}\tau^-\bar{\nu}_\tau)/\mathcal{B}(\bar{B}^0 \to D^{*+}\mu^-\bar{\nu}_\mu)$, Phys. Rev. Lett. **115**, 111803 (2015).

[5] J. P. Lees *et al.* (*BABAR* Collaboration), Measurement of branching fractions and rate asymmetries in the rare decays $B \to K^{(*)}\ell^+\ell^-$, Phys. Rev. D **86**, 032012 (2012).

[6] B. Abi *et al.* (Muon $g-2$ Collaboration), Measurement of the Positive Muon Anomalous Magnetic Moment to 0.46 ppm, Phys. Rev. Lett. **126**, 141801 (2021).

[7] S. Choudhury *et al.* (Belle Collaboration), Test of lepton flavor universality and search for lepton flavor violation in $B \to K^{(*)}\ell\ell$ decays, J. High Energy Phys. 03 (2021) 105.

[8] R. Aaij *et al.* (LHCb Collaboration), Test of lepton universality in beauty-quark decays, Nat. Phys. **18**, 277 (2022).

[9] T. Aaltonen *et al.*, High-precision measurement of the w boson mass with the CDF II detector, Science **376**, 170 (2022).

[10] J. Isaacson, Y. Fu, and C. P. Yuan, RESBOS2 and the CDF W mass measurement, arXiv:2205.02788.

[11] A. Crivellin and M. Hoferichter, Hints of lepton flavor universality violations, Science **374**, 1051 (2021).

[12] A. D'Alise *et al.*, Standard model anomalies: Lepton flavour non-universality and lepton $g-2$, J. High Energy Phys. 08 (2022) 125.

[13] G. Cacciapaglia and F. Sannino, The W boson mass weighs in on the non-standard Higgs, Phys. Lett. B **832**, 137232 (2022).

[14] A. Strumia, Interpreting electroweak precision data including the W-mass CDF anomaly, J. High Energy Phys. 08 (2022) 248.

[15] J. de Blas, M. Pierini, L. Reina, and L. Silvestrini, Impact of the Recent Measurements of the Top-Quark and W-Boson Masses on Electroweak Precision Fits, Phys. Rev. Lett. **129**, 271801 (2022).

[16] C.-T. Lu, L. Wu, Y. Wu, and B. Zhu, Electroweak precision fit and new physics in light of W boson mass, Phys. Rev. D **106**, 035034 (2022).

[17] LHCb Collaboration, Measurement of lepton universality parameters in $B^+ \to K^+\ell^+\ell^-$ and $B^0 \to K^{*0}\ell^+\ell^-$ decays, arXiv:2212.09153.

[18] LHCb Collaboration, Test of lepton universality in $b \to s\ell^+\ell^-$ decays, arXiv:2212.09152.

[19] P. Arnan, A. Crivellin, M. Fedele, and F. Mescia, Generic loop effects of new scalars and fermions in $b \to s\ell^+\ell^-$, $(g-2)_\mu$ and a vector-like 4$^{\text{th}}$ generation, J. High Energy Phys. 06 (2019) 118.

[20] G. Arcadi, L. Calibbi, M. Fedele, and F. Mescia, Systematic approach to B-physics anomalies and t-channel dark matter, Phys. Rev. D **104**, 115012 (2021).

[21] G. Arcadi, L. Calibbi, M. Fedele, and F. Mescia, Muon $g-2$ and B-Anomalies from Dark Matter, Phys. Rev. Lett. **127**, 061802 (2021).

[22] P. Arnan, L. Hofer, F. Mescia, and A. Crivellin, Loop effects of heavy new scalars and fermions in $b \to s\mu^+\mu^-$, J. High Energy Phys. 04 (2017) 043.

[23] L. Calibbi, R. Ziegler, and J. Zupan, Minimal models for dark matter and the muon $g-2$ anomaly, J. High Energy Phys. 07 (2018) 046.

[24] A. Crivellin, M. Hoferichter, and P. Schmidt-Wellenburg, Combined explanations of $(g-2)_{\mu,e}$ and implications for a large muon EDM, Phys. Rev. D **98**, 113002 (2018).

[25] A. Crivellin and M. Hoferichter, Consequences of chirally enhanced explanations of $(g-2)_\mu$ for $h \to \mu\mu$ and $Z \to \mu\mu$, J. High Energy Phys. 07 (2021) 135; 10 (2022) 030(E).

[26] G. Cacciapaglia, C. Cot, and F. Sannino, Naturalness of lepton non-universality and muon $g-2$, Phys. Lett. B **825**, 136864 (2022).

[27] F. Sannino, A. Strumia, A. Tesi, and E. Vigiani, Fundamental partial compositeness, J. High Energy Phys. 11 (2016) 029.

[28] G. Cacciapaglia, H. Gertov, F. Sannino, and A. E. Thomsen, Minimal fundamental partial compositeness, Phys. Rev. D **98**, 015006 (2018).

[29] F. Sannino, P. Stangl, D. M. Straub, and A. E. Thomsen, Flavor physics and flavor anomalies in minimal fundamental partial compositeness, Phys. Rev. D **97**, 115046 (2018).

[30] M. J. Baker, P. Cox, and R. R. Volkas, Radiative muon mass models and $(g-2)_\mu$, J. High Energy Phys. 05 (2021) 174.

[31] M. Cirelli, N. Fornengo, and A. Strumia, Minimal dark matter, Nucl. Phys. **B753**, 178 (2006).

[32] A. Belyaev, G. Cacciapaglia, D. Locke, and A. Pukhov, Minimal consistent dark matter models for systematic experimental characterisation: Fermion dark matter, J. High Energy Phys. 10 (2022) 014.

[33] Alternative scenarios foresee a possible mixing of left- and right-handed components. A second benchmark scenario can be considered with equal couplings to left- and right-handed quarks, i.e., $y_Q^{ij} = y_U^{ij} = y_D^{ij}$. Scenarios where the $y_U^{ij} \neq y_D^{ij} = 0$ will present a different phenomenology and different branching ratios for the decays of $\mathcal{S}_q$ to right-handed up-type and down-type quarks.

[34] A. M. Sirunyan *et al.* (CMS Collaboration), Search for supersymmetry in proton-proton collisions at 13 TeV in final states with jets and missing transverse momentum, J. High Energy Phys. 10 (2019) 244.

[35] A. Tumasyan *et al.* (CMS Collaboration), Combined searches for the production of supersymmetric top quark partners in proton-proton collisions at $\sqrt{s} = 13$ TeV, Eur. Phys. J. C **81**, 970 (2021).

[36] T. Aoyama, M. Hayakawa, T. Kinoshita, and M. Nio, Complete Tenth-Order QED Contribution to the Muon $g-2$, Phys. Rev. Lett. **109**, 111808 (2012).

[37] T. Aoyama, T. Kinoshita, and M. Nio, Theory of the anomalous magnetic moment of the electron, Atoms **7**, 28 (2019).

[38] A. Czarnecki, W. J. Marciano, and A. Vainshtein, Refinements in electroweak contributions to the muon anomalous magnetic moment, Phys. Rev. D **67**, 073006 (2003); **73**, 119901(E) (2006).

[39] C. Gnendiger, D. Stöckinger, and H. Stöckinger-Kim, The electroweak contributions to $(g-2)_\mu$ after the Higgs boson mass measurement, Phys. Rev. D **88**, 053005 (2013).

[40] M. Davier, A. Hoecker, B. Malaescu, and Z. Zhang, Reevaluation of the hadronic vacuum polarisation contributions to the standard model predictions of the muon $g-2$ and $\alpha(m_Z^2)$ using newest hadronic cross-section data, Eur. Phys. J. C **77**, 827 (2017).

[41] A. Keshavarzi, D. Nomura, and T. Teubner, Muon $g-2$ and $\alpha(M_Z^2)$: A new data-based analysis, Phys. Rev. D **97**, 114025 (2018).

[42] G. Colangelo, M. Hoferichter, and P. Stoffer, Two-pion contribution to hadronic vacuum polarization, J. High Energy Phys. 02 (2019) 006.

[43] M. Hoferichter, B.-L. Hoid, and B. Kubis, Three-pion contribution to hadronic vacuum polarization, J. High Energy Phys. 08 (2019) 137.

[44] M. Davier, A. Hoecker, B. Malaescu, and Z. Zhang, A new evaluation of the hadronic vacuum polarisation contributions to the muon anomalous magnetic moment and to $\boldsymbol{\alpha}(m_Z^2)$, Eur. Phys. J. C **80**, 241 (2020); **80**, 410(E) (2020).

[45] A. Keshavarzi, D. Nomura, and T. Teubner, $g-2$ of charged leptons, $\alpha(M_Z^2)$, and the hyperfine splitting of muonium, Phys. Rev. D **101**, 014029 (2020).

[46] A. Kurz, T. Liu, P. Marquard, and M. Steinhauser, Hadronic contribution to the muon anomalous magnetic moment to next-to-next-to-leading order, Phys. Lett. B **734**, 144 (2014).

[47] K. Melnikov and A. Vainshtein, Hadronic light-by-light scattering contribution to the muon anomalous magnetic moment revisited, Phys. Rev. D **70**, 113006 (2004).

[48] P. Masjuan and P. Sanchez-Puertas, Pseudoscalar-pole contribution to the $(g_\mu-2)$: A rational approach, Phys. Rev. D **95**, 054026 (2017).

[49] G. Colangelo, M. Hoferichter, M. Procura, and P. Stoffer, Dispersion relation for hadronic light-by-light scattering: Two-pion contributions, J. High Energy Phys. 04 (2017) 161.

[50] M. Hoferichter, B.-L. Hoid, B. Kubis, S. Leupold, and S. P. Schneider, Dispersion relation for hadronic light-by-light scattering: Pion pole, J. High Energy Phys. 10 (2018) 141.

[51] A. Gérardin, H. B. Meyer, and A. Nyffeler, Lattice calculation of the pion transition form factor with $N_f=2+1$ Wilson quarks, Phys. Rev. D **100**, 034520 (2019).

[52] J. Bijnens, N. Hermansson-Truedsson, and A. Rodríguez-Sánchez, Short-distance constraints for the HLbL contribution to the muon anomalous magnetic moment, Phys. Lett. B **798**, 134994 (2019).

[53] G. Colangelo, F. Hagelstein, M. Hoferichter, L. Laub, and P. Stoffer, Longitudinal short-distance constraints for the hadronic light-by-light contribution to $(g-2)_\mu$ with large-N_c Regge models, J. High Energy Phys. 03 (2020) 101.

[54] T. Blum, N. Christ, M. Hayakawa, T. Izubuchi, L. Jin, C. Jung, and C. Lehner, Hadronic Light-by-Light Scattering Contribution to the Muon Anomalous Magnetic Moment from Lattice QCD, Phys. Rev. Lett. **124**, 132002 (2020).

[55] G. Colangelo, M. Hoferichter, A. Nyffeler, M. Passera, and P. Stoffer, Remarks on higher-order hadronic corrections to the muon $g-2$, Phys. Lett. B **735**, 90 (2014).

[56] T. Aoyama *et al.*, The anomalous magnetic moment of the muon in the standard model, Phys. Rep. **887**, 1 (2020).

[57] C. Alexandrou *et al.*, Lattice calculation of the short and intermediate time-distance hadronic vacuum polarization contributions to the muon magnetic moment using twisted-mass fermions, arXiv:2206.15084.

[58] G. Aad *et al.* (ATLAS Collaboration), A search for the dimuon decay of the standard model Higgs boson with the ATLAS detector, Phys. Lett. B **812**, 135980 (2021).

[59] A. M. Sirunyan *et al.* (CMS Collaboration), Evidence for Higgs boson decay to a pair of muons, J. High Energy Phys. 01 (2021) 148.

[60] CMS Collaboration, Prospects for the precise measurement of the Higgs boson properties in the $H\to\mu\mu$ decay channel at the HL-LHC, CERN Report No. CMS-PAS-FTR-21-004, 2022.

[61] G. D'Amico, M. Nardecchia, P. Panci, F. Sannino, A. Strumia, R. Torre, and A. Urbano, Flavour anomalies after the R_{K^*} measurement, J. High Energy Phys. 09 (2017) 010.

[62] S. Borsanyi *et al.*, Leading hadronic contribution to the muon magnetic moment from lattice QCD, Nature (London) **593**, 51 (2021).

[63] C. T. H. Davies *et al.* (Fermilab Lattice, HPQCD, and MILC Collaborations), Windows on the hadronic vacuum polarisation contribution to the muon anomalous magnetic moment, Phys. Rev. D **106**, 074509 (2022).

[64] M. Cè *et al.*, Window observable for the hadronic vacuum polarization contribution to the muon $g-2$ from lattice QCD, Phys. Rev. D **106**, 114502 (2022).

[65] G. Colangelo, A. X. El-Khadra, M. Hoferichter, A. Keshavarzi, C. Lehner, P. Stoffer, and T. Teubner, Data-driven evaluations of Euclidean windows to scrutinize hadronic vacuum polarization, Phys. Lett. B **833**, 137313 (2022).

[66] T. Aaltonen *et al.* (CDF Collaboration), High-precision measurement of the W boson mass with the CDF II detector, Science **376**, 170 (2022).

[67] P. A. Zyla *et al.* (Particle Data Group), Review of particle physics, Prog. Theor. Exp. Phys. **2020**, 083C01 (2020).

[68] ALEPH, CDF, D0, DELPHI, L3, OPAL, SLD, LEP Electroweak Working Group, Tevatron Electroweak Working Group, SLD Electroweak, and Heavy Flavour Groups Collaborations, Precision electroweak measurements and constraints on the standard model, arXiv:1012.2367.

[69] M. Aaboud *et al.* (ATLAS Collaboration), Measurement of the W-boson mass in pp collisions at $\sqrt{s}=7$ TeV with the ATLAS detector, Eur. Phys. J. C **78**, 110 (2018); **78**, 898(E) (2018).

[70] R. Aaij *et al.* (LHCb Collaboration), Measurement of the W boson mass, J. High Energy Phys. 01 (2022) 036.

[71] G. Altarelli, R. Barbieri, and F. Caravaglios, The epsilon variables for electroweak precision tests: A reappraisal, Phys. Lett. B **349**, 145 (1995).

[72] M. E. Peskin and T. Takeuchi, A New Constraint on a Strongly Interacting Higgs Sector, Phys. Rev. Lett. **65**, 964 (1990).

[73] M. E. Peskin and T. Takeuchi, Estimation of oblique electroweak corrections, Phys. Rev. D **46**, 381 (1992).

[74] D. C. Kennedy and P. Langacker, Precision Electroweak Experiments and Heavy Physics: A Global Analysis, Phys. Rev. Lett. **65**, 2967 (1990); **66**, 395(E) (1991).

[75] H.-J. He, N. Polonsky, and S.-f. Su, Extra families, Higgs spectrum and oblique corrections, Phys. Rev. D **64**, 053004 (2001).

[76] J. Haller, A. Hoecker, R. Kogler, K. Mönig, T. Peiffer, and J. Stelzer, Update of the global electroweak fit and constraints on two-Higgs-doublet models, Eur. Phys. J. C **78**, 675 (2018).